



**HAL**  
open science

## Probing the nuclear symmetry energy with heavy-ion collisions

M Di Toro, V Baran, M Colonna, V Greco

► **To cite this version:**

M Di Toro, V Baran, M Colonna, V Greco. Probing the nuclear symmetry energy with heavy-ion collisions. *Journal of Physics G: Nuclear and Particle Physics*, 2010, 37 (8), pp.83101. 10.1088/0954-3899/37/8/083101 . hal-00600825

**HAL Id: hal-00600825**

**<https://hal.science/hal-00600825>**

Submitted on 16 Jun 2011

**HAL** is a multi-disciplinary open access archive for the deposit and dissemination of scientific research documents, whether they are published or not. The documents may come from teaching and research institutions in France or abroad, or from public or private research centers.

L'archive ouverte pluridisciplinaire **HAL**, est destinée au dépôt et à la diffusion de documents scientifiques de niveau recherche, publiés ou non, émanant des établissements d'enseignement et de recherche français ou étrangers, des laboratoires publics ou privés.

# Probing the Nuclear Symmetry Energy with Heavy Ion Collisions

M Di Toro<sup>1 2</sup>, V Baran<sup>3</sup>, M Colonna<sup>1</sup>, V Greco<sup>1 2</sup>

<sup>1</sup> Laboratori Nazionali del Sud INFN, I-95123 Catania, Italy

<sup>2</sup> Physics and Astronomy Dept., University of Catania

<sup>3</sup> Physics Faculty, Univ. of Bucharest and NIPNE-HH, Romania

E-mail: ditoro@lns.infn.it

## Abstract.

Heavy Ion Collisions (*HIC*) represent a unique tool to probe the in-medium nuclear interaction in regions away from saturation. In this report we present a selection of new reaction observables in dissipative collisions particularly sensitive to the symmetry term of the nuclear Equation of State (*Iso* – *EoS*). We will first discuss the Isospin Equilibration Dynamics. At low energies this manifests via the recently observed Dynamical Dipole Radiation, due to a collective neutron-proton oscillation with the symmetry term acting as a restoring force. At higher beam energies Iso-EoS effects will be seen in an Isospin Diffusion mechanism, via Imbalance Ratio Measurements, in particular from correlations to the total kinetic energy loss. For fragmentation reactions in central events we suggest to look at the coupling between isospin distillation and radial flow. In Neck Fragmentation reactions important *Iso* – *EoS* information can be obtained from fragment isospin content, velocity and alignment correlations.

The high density symmetry term can be probed from isospin effects on heavy ion reactions at relativistic energies (few *AGeV* range), in particular for high transverse momentum selections of the reaction products. Rather isospin sensitive observables are proposed from nucleon/cluster emissions, collective flows and meson production. The possibility to shed light on the controversial neutron/proton effective mass splitting in asymmetric matter is also suggested.

A large symmetry repulsion at high baryon density will also lead to an “earlier” hadron-deconfinement transition in n-rich matter. The binodal transition line of the ( $T, \rho_B$ ) diagram is lowered to a region accessible through heavy ion collisions in the energy range of the new planned facilities, e.g. the *FAIR/NICA* projects. Some observable effects of the formation of a Mixed Phase are suggested, in particular a *Neutron Trapping* mechanism. The dependence of the results on a suitable treatment of the isovector part of the interaction in effective QCD Lagrangian approaches is critically discussed.

We stress the interest of this study in nuclear astrophysics, in particular for supernovae explosions and neutron star structure, where the knowledge of the *Iso* – *EoS* is important at low as well as at high baryon density.

PACS numbers: 21.65.-f, 25.75.Nq, 05.70.Fh, 05.70.Ce, 12.38.Mh

Submitted to: *J. Phys. G: Nucl. Phys.*

## 1. Introduction: The Elusive Symmetry Term of the EoS

The study of the behavior of nuclear matter under several conditions of density and temperature is of crucial importance for the understanding of a large variety of phenomena, ranging from the structure of nuclei and their decay modes, up to the life and the properties of massive stars. Mechanisms involving an enormous range of scales in size, characteristic time and energy, but all based on nuclear processes at fundamental level, are actually linked by the concept of the nuclear Equation of State (*EoS*) and the associated energy density functional. In particular, the understanding of the properties of exotic nuclei, as well as neutron stars and supernova dynamics, entails constraining the behavior of the nuclear symmetry energy, which describes the difference between the binding energy of symmetric matter (with equal proton and neutron numbers,  $N=Z$ ), and that of pure neutron matter.

Transient states of nuclear matter far from normal conditions can be created in terrestrial laboratories via Heavy Ion Collisions (*HIC*). Many experimental and theoretical efforts have been devoted, over the past 30 years, to the study of nuclear reactions from low to intermediate energies, as a possible tool to learn about the behavior of nuclear matter and its *EoS*. Relevant conclusions have been reached concerning the *EoS* of symmetric matter for densities up to five times the saturation value [23]. More recently, the availability of neutron-rich and exotic beams has opened the way to investigate, in laboratory conditions, new aspects of nuclear structure and dynamics up to extreme ratios of neutron to proton numbers. Thus it has become possible to explore the behavior of nuclear matter along a new degree of freedom, the asymmetry  $I = (N - Z)/(N + Z)$  (in the rest of the review also defined as  $\beta$  or  $\alpha$ ), aiming at constraining the density and/or temperature dependence of the symmetry energy (*Iso* – *EoS*). Here we will review the Isospin Dynamics in *HIC* from the Coulomb Barrier to Relativistic Energies.

The symmetry energy  $E_{sym}$  appears in the energy density  $\epsilon(\rho, \rho_3) \equiv \epsilon(\rho) + \rho E_{sym}(\rho_3/\rho)^2 + O(\rho_3/\rho)^4 + \dots$ , expressed in terms of total ( $\rho = \rho_p + \rho_n$ ) and isospin ( $\rho_3 = \rho_p - \rho_n$ ) densities [1]. The symmetry term gets a kinetic contribution directly from basic Pauli correlations and a potential part from the highly controversial isospin dependence of the effective interactions. Both at sub-saturation and supra-saturation densities, predictions based on the existing many-body techniques diverge rather widely, see [2, 3, 4]. We recall that the knowledge of the *EoS* of asymmetric matter is very important at low densities, in nuclear structure (neutron skins, pigmy resonances, refs. [5, 6, 7, 8]), in reactions (neutron distillation in fragmentation [9], charge equilibration [10]), in astrophysics (neutron star formation and crust, [11, 12]) as well as at high densities in relativistic heavy ion reactions (isospin flows [13], particle production [1, 14, 15, 16]), in compact star (neutron star mass-radius relation, cooling, hybrid structure, formation of black holes, [17, 18, 19, 20]) and for fundamental properties of strong interacting systems (transition to new phases of the matter, [21, 22]).

Several observables which are sensitive to the *Iso* – *EoS* and testable experimentally,

have been suggested [1, 14, 24, 25, 26, 27, 28, 29, 30]. We take advantage of new opportunities in theory (development of rather reliable microscopic transport codes for *HIC*) and in experiments (availability of very asymmetric radioactive beams, improved possibility of measuring event-by-event correlations) to present new results that are constraining the existing effective interaction models. We will discuss dissipative collisions in a wide range of beam energies, from just above the Coulomb barrier up to the *AGeV* range. Isospin effects on the chiral/deconfinement transition at high baryon density will be also analyzed. Low to Fermi energies will bring information on the symmetry term around (below) normal density, while intermediate energies will probe high density regions. The transport codes are based on mean field theories, with correlations included via hard nucleon-nucleon elastic and inelastic collisions and via stochastic forces, selfconsistently evaluated from the mean phase-space trajectory, see [1, 31, 32, 33]. Stochasticity is essential in order to get distributions as well as to allow the growth of dynamical instabilities.

Relativistic collisions are described via a fully covariant transport approach, related to an effective field exchange model, where the relevant degrees of freedom of the nuclear dynamics are accounted for [1, 15, 16, 34, 35, 36]. We will have a propagation of particles suitably dressed by self-energies that will influence collective flows and in medium nucleon-nucleon inelastic cross sections. The construction of an *Hadron – EoS* at high baryon and isospin densities will finally allow the possibility of developing a model of a hadron-deconfinement transition at high density for an asymmetric matter [22]. The problem of a correct treatment of the isospin in an effective partonic *EoS* will be stressed.

It is clear that using quasiparticle transport approaches we will not properly address the problem of symmetry energy at very low densities, below  $\rho/\rho_0 = 0.1$ , with  $\rho_0$  saturation density, where the mean field picture will break down. The relevance of cluster formation via many-body correlations has been clearly shown to determine the symmetry term in such highly diluted asymmetric matter, [37, 38]. It is nice to note that a smooth transition is expected to the mean field predictions at higher densities discussed in this review [38], where in fact clusterization is still described by extended one-body approaches, via spinodal instabilities, see Sect.4.2.

## 2. The Stochastic Mean Field transport approach

At low to intermediate energies the evolution of systems governed by a complex phase space can be described via a transport equation (of the Boltzmann-Nordheim-Vlasov type) with a fluctuating term, the so-called Boltzmann-Langevin equation (BLE) [1]

$$\frac{df}{dt} = \frac{\partial f}{\partial t} + \{f, H\} = I_{coll}[f] + \delta I[f], \quad (1)$$

where  $f(\mathbf{r}, \mathbf{p}, t)$  is the one-body distribution function, or Wigner transform of the one-body density,  $H(\mathbf{r}, \mathbf{p}, t)$  the mean field Hamiltonian,  $I_{coll}$  the two-body collision term (that accounts for the residual interaction) incorporating the Fermi statistics of the

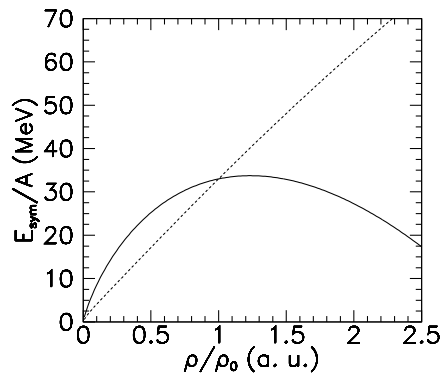


**Figure 1.** Density dependence of the symmetry energies used in the simulations presented here: Asy-soft (solid) and Asy-stiff (dashed).

particles, and  $\delta I[f]$  the fluctuating part of the collision integral [39, 40]. The system is described in terms of the one-body distribution function  $f$ , however this function may experience a stochastic evolution in response to the action of the fluctuating term  $\delta I[f]$ . This is an effective way to insert again into the dynamics the effects of unknown correlations and of the loss of information caused by the projection of the many-body dynamics onto a much reduced subspace. Here we will follow the approximate treatment to the BLE presented in Refs.[31, 32], the Stochastic Mean Field (SMF) model, that consists in the implementation of stochastic spatial density fluctuations. The nuclear EoS, directly linked to the mean-field Hamiltonian  $H$ , can be written as:

$$\frac{E}{A}(\rho, I) = \frac{E}{A}(\rho) + E_{sym}(\rho)I^2 + O(I^4) \quad (2)$$

We adopt a soft isoscalar EOS,  $E/A(\rho)$ , with compressibility modulus  $K = 220 \text{ MeV}$ , which is favored from monopole oscillations in stable nuclei as well as from flow studies [23].

We will always test the sensitivity of our simulation results to different choices of the density and momentum dependence of the Isovector part of the Equation of State (*Iso - EoS*). In the non-relativistic frame the potential part of the symmetry energy,  $C_{sym}(\rho)$ , [1]:

$$E_{sym} = E_{sym}(kin) + E_{sym}(pot) \equiv \frac{\epsilon_F}{3} + C_{sym}(\rho) \quad (3)$$

is tested by employing three different density parametrizations of the symmetry potentials [1, 24, 41], one with a rapidly increasing behaviour with density, roughly proportional to  $\rho^2$  (*Asy - superstiff*), one with a linear increase of the potential part of the symmetry energy with density (*Asy - stiff*) and one with a kind of saturation around normal density (*Asy - soft*), even decreasing at higher densities.

In particular, for the symmetry term with the stronger density dependence,

$$E_{sym}(\rho) = a \cdot \left(\frac{\rho}{\rho_0}\right)^{2/3} + b \cdot \frac{2(\rho/\rho_0)^2}{1 + (\rho/\rho_0)}, \quad (4)$$

where  $\rho_0$  is the saturation density,  $a=12.7$  MeV (fixed by the kinetic contribution Eq.3) and  $b=19$  MeV, to give a saturation value of  $31.7$  MeV. The linear density dependence is simply given by:

$$E_{sym}(\rho) = a \cdot \left(\frac{\rho}{\rho_0}\right)^{2/3} + b \cdot (\rho/\rho_0), \quad (5)$$

For the symmetry term with weaker density dependence around saturation

$$E_{sym}(\rho) = a \cdot \left(\frac{\rho}{\rho_0}\right)^{2/3} + 240.9\rho - 819.1\rho^2, \quad (6)$$

where  $a=12.7$  MeV.

The three parameterizations cross at normal density at the empirically known symmetry energy coefficient of the Bethe-Weizsäcker formula. As shown in Fig.1 the symmetry energy at densities below the normal value is larger in the Asysoft case, while above saturation it is higher in the Asystiff cases. Hence in the low-density regime, that is the region of interest for our analysis in heavy ion collisions at Fermi energies, isospin effects are expected to be stronger in the Asysoft case. Opposite expectations can be derived for relativistic collisions, where high density regions will be probed in the early stage of the collision. In any case, for mechanisms sensitive to the density derivative of the symmetry energy an Asystiff-like behavior is more effective.

### 2.1. Momentum Dependence of the Symmetry Potentials

A particular attention is devoted to the isospin effects on the momentum dependence of the symmetry potentials, i.e. to observables sensitive to a different neutron/proton effective mass in asymmetric matter. The problem of Momentum Dependence in the Isovector channel (*Iso - MD*) is still very controversial and it would be extremely important to get more definite experimental information, see the refs. [1, 14, 42, 43]. Exotic beams at intermediate energies are of interest in order to have high momentum particles and to test regions of high baryon (isoscalar) and isospin (isovector) density during the reaction dynamics.

Our transport code has been implemented with a generalized form of the effective interactions, which can be easily reduced to Skyrme-like forces, with momentum dependent terms also in the isovector channel [43, 44, 45, 46], i.e. with a different  $(n, p)$  mean field momentum dependence. The general structure of the isoscalar and isovector Momentum Dependent (MD) effective fields is derived via an isospin asymmetric extension of the Gale-Bertsch-DasGupta (GBD) force [47, 48, 49, 50, 51], which corresponds to a Yukawian non-locality. The isovector momentum dependence implies different effective masses for protons and neutrons given as  $\frac{m_\tau^*}{m} = (1 + \frac{m}{\hbar^2 p} \frac{\partial U_\tau}{\partial p})^{-1}$ , for  $p = p_{F,\tau}$ , at fixed density. Thus our approach will allow to follow the dynamical effect of opposite  $n/p$  effective mass splitting while keeping the same density dependence of the symmetry energy [46, 52].

In fact when we use momentum-dependent interactions we have also contributions to the symmetry energy from the non-local terms. This is shown in Fig.2 where we plot

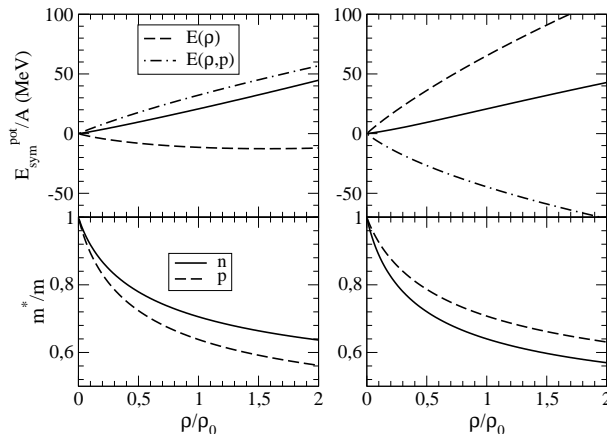


**Figure 2.** Upper Panels: Density dependence of the potential symmetry energy (Solid Lines), in the *Asystiff* choice. Dashed lines refer to local contributions, dot-dash lines to momentum-dependent ones, see text. Left:  $m_n^* > m_p^*$  parametrization; Right:  $m_n^* < m_p^*$  case. Lower Panels: corresponding behavior of neutron/proton effective masses as a function of the density, for an asymmetry  $\beta = 0.2$ .

the density dependence of the potential part of the symmetry energy, in the Asy-stiff case, for the two choices of the n/p mass splitting (solid lines, upper panels). We also separately report the contributions from the momentum-dependent,  $E(\rho, p)$ , and the density dependent,  $E(\rho)$ , part of the EoS, whose sum gives the total  $E_{sym}^{pot}$  (the  $C_{sym}(\rho)$  of Eq.(3)). A change in the sign of the mass splitting is related to opposite behaviors of these two contributions, exactly like it happens in Skyrme-like forces, see sections (2.1-2.2) of ref.[1]. The lower panels show the density dependence of the corresponding mass splitting, for an asymmetry parameter  $\beta = 0.2$  (the  $^{197}\text{Au}$  asymmetry). In order to probe the mass splitting effects on the heavy ion dynamics we have chosen parametrizations that give almost opposite splittings at all densities.

In Fig.3 we present the density dependence of the neutron/proton symmetry potentials, for the two stiffnesses of the symmetry term, evaluated in the case without momentum dependence (dashed lines) and in the momentum dependence (*Iso* – *MD*) case for the  $m_n^* < m_p^*$  (dotted) and the opposite  $m_n^* > m_p^*$  (solid) choices. We see that the momentum dependence modifies the effect of the symmetry term stiffness on the nucleon potentials, with differences that become more appreciable with increasing nucleon momenta. From this figure we can already predict large effects of the effective mass splitting at high momenta.

This is shown more explicitly in Fig.4 where we see the momentum dependence of the neutron-proton potentials at saturation density for the two mass splitting choices, always for a "typical"  $\beta = 0.2$  asymmetry ( $^{124}\text{Sn}, ^{197}\text{Au}...$ ). The plot is for the *Asysoft* (left panel) and the *Asystiff* (right) symmetry term, and in fact it is not much different. Indeed we can see also from the previous Fig.3 that at normal density the difference between neutron and proton potentials is almost the same for the two asy-stiffnesses,

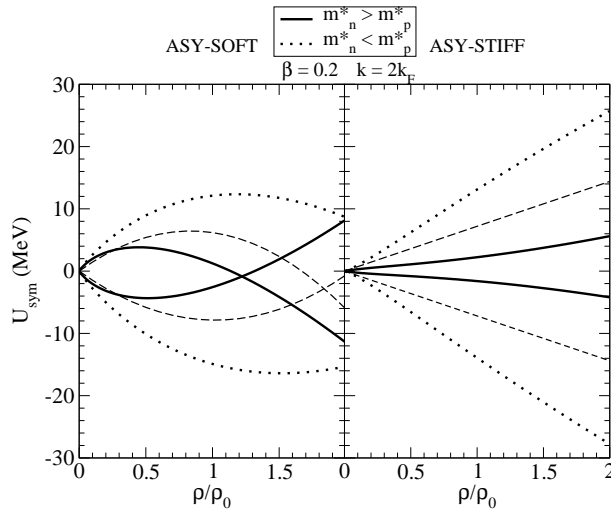


**Figure 3.** Density dependence of neutron(upper)-proton(lower) potentials for an asymmetry  $\beta = 0.2$  for the *Asysoft*(left) and *Asystiff*(right) choices. Dashed: No momentum dependence. Momentum dependent potentials at  $k = 2k_F$ : solid lines for the  $m_n^* > m_p^*$  case, dotted lines for the opposite  $m_n^* < m_p^*$  choice.

even in the case of *Iso* – *MD* interactions..

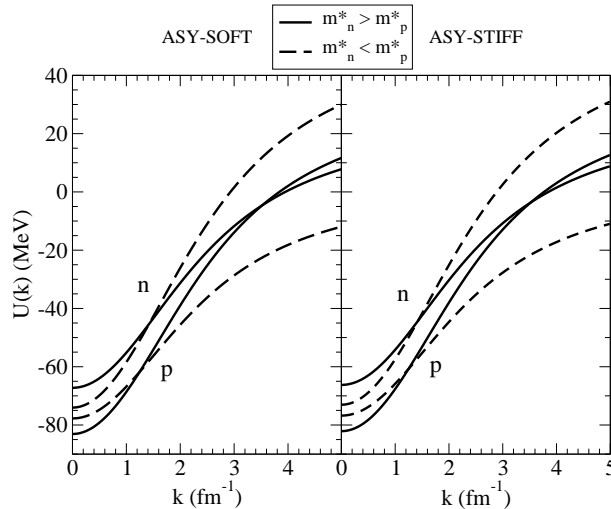


**Figure 4.** Momentum dependence of neutron-proton potentials at saturation density and asymmetry  $\beta = 0.2$ , for the two splitting choices  $m_n^* < m_p^*$  (dashed) and  $m_n^* > m_p^*$  (solid). Left panel: *Asysoft Iso* – *Eos*. Right panel: *Asystiff* case

The Figs.3 and 4 suggest the presence of interesting Isoscalar and Isovector *MD* effects on the reaction dynamics:

- *Isoscalar*. In general the momentum dependence gives more attractive potentials at low momenta,  $p < p_F$ , and more repulsive at high  $p$ ,  $p > p_F$ . In the reaction dynamics we expect the more energetic nucleons to be fast emitted and to suffer less collisions [47]. As a consequence we will have less stopping of the matter and less

compression. The isoscalar EoS becomes stiffer when the momentum dependence is included.

- *Isovector*. Isospin effects on the momentum dependence imply different slopes around  $p_F$  for neutrons and protons, as clearly shown in Fig.4, and so the larger repulsion above  $p_F$  is different. In the case  $m_n^* < m_p^*$  the high momentum neutrons will see a more repulsive field with respect to the high- $p$  protons. The opposite will happen in the  $m_n^* > m_p^*$  case. The fast nucleon emission will be directly affected: in the  $m_n^* < m_p^*$  case we expect a larger  $n/p$  yield for nucleons emitted in central collisions and a larger neutron *Squeeze – out* (elliptic flow) in semicentral collisions in heavy ion reactions at intermediate energies, in particular for high  $p_t$  (transverse momentum) selections. In fact in the interacting, high density, early stage of the reaction dynamics the pressure is built from violent nucleon-nucleon collisions and the high  $p_t$  particles will carry the maximal information on high density and momentum dependence of the symmetry potentials. The azimuthal distributions (elliptic flows) will be particularly affected since particles mostly retain their high transverse momenta escaping along directions orthogonal to the reaction plane without suffering much rescattering processes.

In Sect.5 we will test those predictions also for n-rich vs. n-poor light ions, like ( $^3H$ ,  $^3He$ ), easier to detect. Since, as already noted, the symmetry potentials are not very different in the *Asystiff/Asysoft* choice for the density range probed at intermediate energies, we can expect that the *Mass – Splitting* effect could be even larger than the one related to the different stiffness of the symmetry term.

### 3. Isospin Equilibration in Low Energy Dissipative Collisions

The presence of an Isovector Dipole Oscillation in the entrance channel dynamics has been suggested by several authors in order to account for the fast charge equilibration, and even for the fragment charge distributions, in Deep Inelastic Collisions [53, 54, 55, 56, 57, 58]. Since the oscillation is triggered by the mean field of a dilute Dinuclear Composite System this mechanism seems to appropriate for the study of the symmetry term below saturation, which is acting as a restoring force. A direct observation of the corresponding radiative emission would be then interesting. In fact the clear dynamical features of such *pre-equilibrium* dipole mode (large deformations of the source, preferential oscillation on the reaction plane) will allow to distinguish this radiation from the  $\gamma$ -emission of the statistical Giant Dipole Resonances (*GDR*) of the final excited reaction products.

#### 3.1. The Prompt Dipole $\gamma$ -Ray Emission

The possibility of an entrance channel collective dipole, and corresponding radiation, due to an initial different N/Z distribution was predicted at the beginning of the nineties [59, 60]. After several experimental evidences, in fusion as well as in deep-inelastic

reactions, [61, 62] and refs. therein, we have now a good understanding of the process and stimulating new perspectives from the use of radioactive beams, to enhance the sensitivity to the *Iso - EoS*.

In the first stages of dissipative reactions between colliding ions with different  $N/Z$  ratios, a large amplitude dipole collective motion develops in the mean field of the composite dinuclear system, the so-called Dynamical Dipole mode. This gives rise to a prompt  $\gamma$ -ray emission which depends: i) on the absolute value of the initial dipole moment

$$D(t=0) = \frac{NZ}{A} |R_Z(t=0) - R_N(t=0)| = \frac{R_P + R_T}{A} Z_P Z_T \left| \left(\frac{N}{Z}\right)_T - \left(\frac{N}{Z}\right)_P \right|, \quad (7)$$

being  $R_Z = \frac{\sum_i x_i(p)}{Z}$  and  $R_N = \frac{\sum_i x_i(n)}{N}$  the center of mass of protons and of neutrons respectively, while  $R_P$  and  $R_T$  are the projectile and target radii; ii) on the fusion/deep-inelastic dynamics, which rules the formation of the dinuclear mean field; iii) on the symmetry term, below saturation, that is acting as a restoring force. A detailed description can consistently be obtained in mean field transport approaches, [63, 64, 65, 66, 67]. We can follow the time evolution of the dipole moment in the  $r$ -space,  $D(t) = \frac{NZ}{A}(R_Z - R_N)$  and in  $p$ -space,  $DK(t) = (\frac{P_p}{Z} - \frac{P_n}{N})$ , with  $P_p$  ( $P_n$ ) center of mass in momentum space for protons (neutrons), just the canonically conjugate momentum of the  $D(t)$  coordinate, i.e. as operators  $[D(t), DK(t)] = i\hbar$  [67]. A nice "spiral-correlation" clearly denotes the collective nature of the mode, see Fig.5 We can directly apply a bremsstrahlung approach, to the dipole evolution given from the Landau-Vlasov transport [66], to estimate the "prompt" photon emission probability ( $E_\gamma = \hbar\omega$ ):

$$\frac{dP}{dE_\gamma} = \frac{2e^2}{3\pi\hbar c^3 E_\gamma} |D''(\omega)|^2, \quad (8)$$

where  $D''(\omega)$  is the Fourier transform of the dipole acceleration  $D''(t)$ . We remark that in this way it is possible to evaluate, in *absolute* values, the corresponding pre-equilibrium photon emission.

In a recent experiment the prompt dipole radiation has been investigated with a  $4\pi$  gamma detector. A strong dipole-like photon angular distribution ( $\theta_\gamma$ ) =  $W_0[1 + a_2 P_2(\cos\theta_\gamma)]$ ,  $\theta_\gamma$  being the angle between the emitted photon and the beam axis, has been observed, with the  $a_2$  parameter close to  $-1$ , see [62]. At higher beam energies we expect a decrease of the direct dipole radiation for two main reasons both due to the increasing importance of hard NN collisions: i) a larger fast neutron emission that will equilibrate the isospin during the dipole oscillation; ii) a larger damping of the collective mode due to  $np$  collisions.

The use of unstable neutron rich projectiles would largely increase the effect, due to the possibility of larger entrance channel asymmetries [68]. In order to suggest proposals for the new *RIB* facility *Spiral 2*, [69] we have studied fusion events in the reaction  $^{132}\text{Sn} + ^{58}\text{Ni}$  at  $10\text{AMeV}$ , [68, 70]. We expect a *Monster* Dynamical Dipole, the initial dipole moment  $D(t=0)$  being of the order of 50fm, about two times the largest values

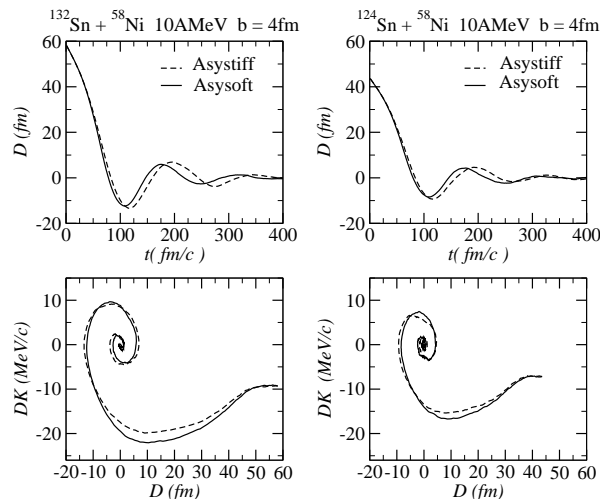


**Figure 5.** Dipole Dynamics at 10 A MeV,  $b = 4$  fm centrality. Left Panels: Exotic “132” system. Upper: Time evolution of dipole moment  $D(t)$  in real space; Lower: Dipole phase-space correlation (see text). Right Panels: same as before for the stable “124” system. Solid lines correspond to Asy-soft EoS, the dashed to Asy-stiff EoS.

probed so far, allowing a detailed study of the symmetry potential, below saturation, responsible of the restoring force of the dipole oscillation and even of the damping, via the fast neutron emission.

In Fig. 5 we report some global informations concerning the dipole mode in entrance channel. In the Left-Upper panel we have the time evolution of the dipole moment  $D(t)$  for the “132” system at  $b = 4$  fm. We notice the large amplitude of the first oscillation but also the delayed dynamics for the Asy-stiff EoS related to a weaker isovector restoring force.

The phase space correlation (spiraling) between  $D(t)$  and  $DK(t)$ , is reported in Fig.5 (Left-Lower). It nicely points out a collective behavior which initiates very early, with a dipole moment still close to the touching configuration value reported above. This can be explained by the fast formation of a well developed neck mean field which sustains the collective dipole oscillation in the dinuclear configuration.

The role of a large charge asymmetry between the two colliding nuclei can be seen from Fig.5 (Right Panels), where we show the analogous dipole phase space trajectories for the stable  $^{124}\text{Sn} + ^{58}\text{Ni}$  system at the same value of impact parameter and energy. A clear reduction of the collective behavior is evidenced.

In Fig.6 (Left Panel) we report the power spectrum,  $|D''(\omega)|^2$  in semicentral “132” reactions, for different *Iso – EoS* choices. The gamma multiplicity is simply related to it, see Eq.(8). The corresponding results for the stable “124” system are drawn in the Right Panel. As expected from the larger initial charge asymmetry, we clearly see an increase of the Prompt Dipole Emission for the exotic n-rich beam. Such entrance channel effect will be enhanced, allowing a better observation of the Iso-EoS dependence.

We recall that in the Asystiff case we have a weaker restoring force for the dynamical dipole in the dilute “neck” region, where the symmetry energy is smaller [1]. This is

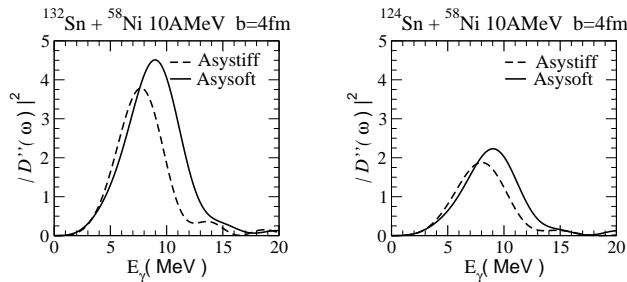


**Figure 6.** Left Panel, Exotic “132” system. Power spectra of the dipole acceleration at  $b = 4\text{fm}$  (in  $c^2$  units). Right Panel: Corresponding results for the stable “124” system. Solid lines correspond to Asysoft EoS, the dashed to Asystiff EoS.

reflected in lower values of the centroids as well as in reduced total yields, as shown in Fig.6. The sensitivity of  $\omega_0$  to the stiffness of the symmetry energy will be amplified by the increase of  $D(t_0)$  when we use exotic, more asymmetric beams.

The prompt dipole radiation angular distribution is the result of the interplay between the collective oscillation life-time and the dinuclear rotation. In this sense we also expect a sensitivity to the  $Iso - EoS$  of the anisotropy, in particular for high spin event selections. E.g. we remind that in the Asy-stiff case we have a delayed onset of the collective dipole (see Fig.5), the emitting system will get more rotation and the angular anisotropy will be reduced [71].

In the Asysoft choice we expect also larger widths of the “resonance” due to the larger fast neutron emission. We note the opposite effect of the Asy-stiffness on neutron vs proton emissions. The latter point is important even for the possibility of an independent test just measuring the  $N/Z$  of the pre-equilibrium nucleon emission, [72, 73].

In general the collective dipole mechanism for charge equilibration will be important in a limited range of beam energies [66]. We must be well above the Coulomb Barrier in order to have a fast formation of the dinuclear mean field, but when the direct nucleon-nucleon collisions will be more frequent we expect a rapid quenching of the isovector collective mode. In Sect.4 we will discuss charge equilibration at the Fermi energies, in a kind of overdamped regime. The mechanism is now based on the isospin diffusion, on a time scale again ruled by the symmetry term at sub-saturation density.

#### 4. Probing the symmetry energy in nuclear reactions in the Fermi energy domain

Heavy ion collisions (*HIC*) in the Fermi energy domain (30-100 AMeV) are dominated by fragmentation mechanisms. After moderate compression effects during the first stage of the collision, the composite nuclear system expands and eventually separates into fragments, whose multiplicity and characteristics depend on the centrality of the reaction. However, as we will illustrate in the following, regardless of the possible different outcomes, fragment properties are always closely linked to the development of

density gradients along the reaction path. In the energy range considered, the properties of nuclear matter below normal density are mostly concerned, allowing one to investigate the low density behavior of the symmetry energy.

In central collisions, where the full disassembly of the system into many intermediate mass fragments (IMF) and particles is observed, one can study specifically properties of liquid-gas phase transitions occurring in asymmetric matter in the presence of radial flow. In neutron-rich matter in the coexistence region one expects to observe isospin distillation: fragments (liquid) appear more symmetric with respect to the initial matter, while light particles (gas) are more neutron-rich [1, 33, 74, 75, 76, 77]. The magnitude of this effect depends on characteristic properties of the isovector sector of the EOS namely on the value and the slope of the symmetry energy at low density [1, 29]. Moreover, interesting correlations between fragment isotopic content and collective velocity can be evidenced, also sensitive to the symmetry energy.

Increasing the impact parameter, fragmentation of the neck region, that is the overlap region between the two colliding nuclei, takes place. In this situation, corresponding to mid-peripheral events, fragment kinematical properties may keep a memory of the entrance channel. The presence of a density gradient between the dilute neck region and the remaining matter, projectile- and target-like fragments (PLF-TLF), induces interesting isospin effects: The IMF's emerging from the neck region are more neutron rich and this 'isospin migration' mechanism is sensitive to the symmetry energy. For more peripheral events one essentially observes a binary outcome, with the possibility of a dynamically induced fast fission, still triggered by the dynamics of the overlap zone. In reactions between systems with different initial  $N/Z$ , isospin diffusion may occur through the low density interface, governed by the strength of the symmetry energy below saturation.

From one side, these arguments lead us to single out the isospin signal as a good tracer of the reaction mechanism [86]. In fact the new features appearing in neutron rich matter can be used to validate our current interpretation of the fragmentation mechanisms. On the other hand, isotopic properties and new correlations, once confronted with experimental data, can be used to probe the symmetry term of the EoS at sub-saturation density.

#### 4.1. Low Density Behavior of $C_{sym}$ : Isospin Diffusion

In this subsection we focus on the mechanisms connected to isospin transport in binary events at Fermi energies. We consider semi-peripheral reactions between systems having different  $N/Z$  and we investigate the diffusion of the initial  $N/Z$  gradient under the conditions dictated by the underlying dynamical evolution. This process involves nucleon exchange through the low density neck region and hence it is sensitive to the low density behavior of  $C_{sym}$ , i.e. of the potential part of the symmetry energy, [10, 46, 78].

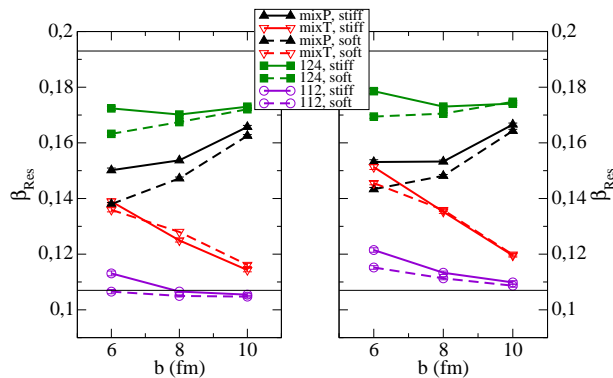


**Figure 7.** (color online) Asymmetries of the residues in  $Sn + Sn$  collisions at incident energies of  $E = 50 A MeV$  (left) and  $35 A MeV$  (right) for MD interactions. Primary fragments at the *freeze-out*.

*4.1.1. Asymmetries of Reaction Components* As a direct consequence of the fact that isospin transport takes place, projectile-like (PLF) and target-like (TLF) fragments, i.e. the sizeable fragments emerging from (mid-)peripheral reactions, have different asymmetries with respect to the initial conditions. This will be illustrated in the case of different  $Sn + Sn$  ( $N/Z = 1.48$  and  $1.24$ ) reactions ( $^{124}Sn + ^{124}Sn$  (HH),  $^{112}Sn + ^{112}Sn$  (LL) and the mixed  $^{124}Sn + ^{112}Sn$  (HL)), for the impact parameters  $b = 6, 8,$  and  $10 fm$  and for two incident energies, 35 and 50 A MeV. This investigation is undertaken performing SMF simulations, with a momentum dependent (MD) isoscalar effective interaction (GBD) [46]. To check whether the isoscalar sector of the interaction may influence isospin effects, we also consider calculations without momentum dependence. In the latter case we employ a momentum independent (MI) Skyrme interaction having the same compressibility modulus as the GBD interaction. As far as the iso-EoS is concerned, calculations are carried out for two symmetry energy parametrizations: Asysoft and Asystiff.

Results are reported in Fig.7, for the MD interaction, the two Iso-EoS and the two incident energies. It is observed that the asymmetry of the residues for the mixed *HL* system decreases for the *n*-rich (PLF) and increases for the *n*-poor (TLF) partner with respect to the initial asymmetries, as expected for isospin equilibration. In the case of the *HH* and *LL* symmetric collisions, we cannot have isospin transport and the only variations come from nucleon emissions, that leads to a reduction of the initial asymmetry. The impact parameter dependence clearly shows that Iso-EoS effects are more relevant for more dissipative collisions, i.e. for smaller impact parameters and thus for longer interaction times. With respect to different Iso-EoS's, we notice that pre-equilibrium emission is more asymmetric for the soft Iso-EoS, which is expected because of the higher symmetry energy and thus the larger neutron repulsion.

Comparing the results obtained at the two incident energies, 50 A MeV (left) and 35 A MeV (right panel), one can see that the neutron emission to the continuum is lower at the lower energy, leading to more initial asymmetric residues. On the other hand the

interaction time is larger in this case, leading to more equilibration in the mixed system.

*4.1.2. Imbalance Ratio* Within a first order approximation of the transport dynamics, the relaxation of a given observable  $x$  towards its equilibrium value can be expressed as:  $x_{P,T}(t) - x^{eq} = (x^{P,T} - x^{eq}) e^{-t/\tau}$ , where  $x^{P,T}$  is the  $x$  value for the projectile (P) or the target (T) before the diffusion takes place,  $x^{eq} = (x^P + x^T)/2$  is the full equilibrium value,  $t$  is the elapsed time and  $\tau$  is the relaxation time, that depends on the mechanism under study. The degree of isospin equilibration reached in the collision can be inferred by looking at isospin dependent observables in the exit channel, such as the asymmetries of PLF and TLF, as discussed above. It is rather convenient to construct the so-called imbalance ratio [10, 86, 87]:

$$R_{P,T}^x = (x_{P,T} - x^{eq}) / |x^{P,T} - x^{eq}| \quad (9)$$

Clearly, this observable measures the difference between the actual asymmetry of PLF (or TLF) and the full equilibrium value, normalized to the initial distance (i.e. to the conditions before the diffusion process has started). In the calculations the latter can be evaluated by looking at the asymmetries of PLF (or TLF), as obtained in the symmetric reactions HH and LL (where diffusion does not take place), after pre-equilibrium nucleon emission is over, see Fig.7. The ratio  $R$  is  $\pm 1$  in the projectile and target regions, respectively, for complete transparency, while it is zero for full equilibration.

Within our approximation, the imbalance ratio simply reads  $R_{P,T} = \pm e^{-t/\tau}$  and is actually independent of the initial asymmetry distance between the reaction partners. Hence it isolates the effects of the isodiffusion mechanism, whose strength is determined by the relaxation time  $\tau$ , related to the symmetry energy. However the degree of equilibration reached in the reaction crucially depends also on the contact time  $t$ , i.e. on the reaction centrality.

From the asymmetries shown before (Fig.7) one can build the imbalance ratios, according to Eq.(9), that are shown in Fig.8, Left Panels, for MD calculations (circles), for the incident energy of 50  $AMeV$  (left) and 35  $AMeV$  (right). Results for stiff and soft Iso-EoS are represented with solid and dashed lines, and those for the projectile and target rapidity regions with full and open symbols (upper and lower curves), respectively. We show also results obtained in the case of the MI interaction (squares).

The equilibration is larger ( $R$  smaller) both for lower energies (right) and for MI interactions (dashed curves). In fact in both cases the reaction is slower and thus the interaction time longer, leading to more equilibration; for the lower energy because of the slower speed, and for the MI interaction because of the less repulsive isoscalar mean field. In comparing the two Iso-EoS's we see that the equilibration is larger for the soft Iso-EoS, since the higher symmetry energy leads to a larger diffusion contribution to the isospin current.

To isolate isospin effects, one could study the asymmetry imbalance ratio as a function of the interaction time (or of an observable directly related to it).

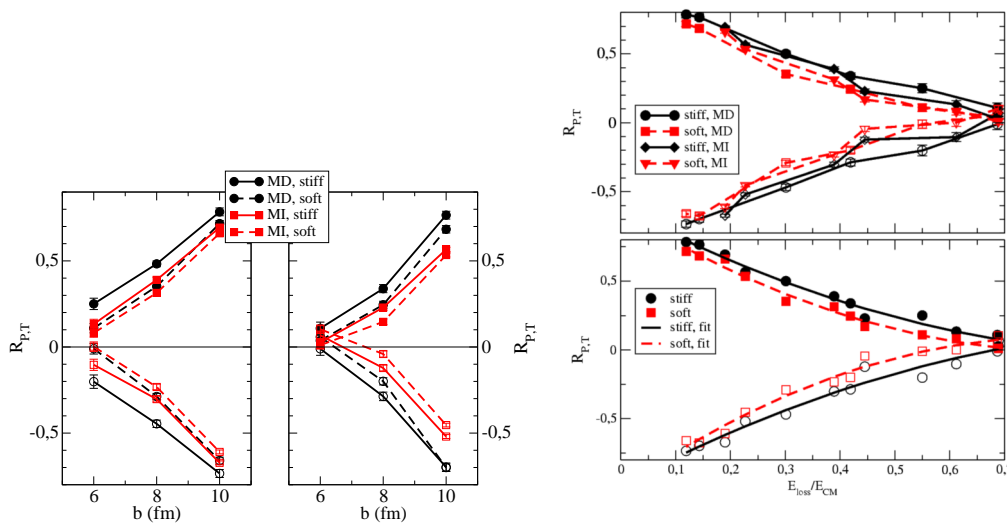


**Figure 8.** (color online) Left Panel. Imbalance ratios for  $Sn+Sn$  collisions for incident energies of 50 (left) and 35  $AMeV$  (right) as a function of the impact parameter. Signatures of the curves: iso-EoS stiff (solid lines), soft (dashed lines); MD interaction (circles), MI interaction (squares); projectile rapidity ( full symbols, upper curves ), target rapidity ( open symbols, lower curves ). Right Panel. Imbalance ratios as a function of relative energy loss for both beam energies. Upper: Separately for stiff (solid) and soft (dashed) iso-EoS, and for MD (circles and squares) and MI (diamonds and triangles) interactions, in the projectile region (full symbols) and the target region (open symbols). Lower: Quadratic fit to all points for the stiff (solid), resp. soft (dashed) iso-EoS.

To this purpose we propose to study the correlations between isospin equilibration and the kinetic energy loss, that is adopted as a selector of the reaction centrality and, hence, of the contact time  $t$ . We define the kinetic energy loss per particle as

$$E_{loss} = E_{cm} - \frac{E_{kin}}{A_{PLF} + A_{TLF}}, \quad E_{cm} = \frac{E_{lab}}{A_P} \frac{A_P A_T}{(A_P + A_T)^2}, \quad (10)$$

where  $A_P, A_T, A_{PLF}, A_{TLF}$  are the masses of the initial projectile and target, and of the final projectile-like and target-like fragments, respectively. Here  $E_{cm}$  is the initial energy, per nucleon, available in the  $cm$  system.  $E_{kin}$  is the final total kinetic energies of the fragments in the  $cm$  system. We mention that the study of isospin equilibration as a function of the heavy residue excitation energy (related to the kinetic energy loss) was suggested in Ref. [80]. In Fig.8, Right Panels, we report the correlation between  $R_{P,T}$  and the total kinetic energy loss (normalized to  $E_{cm}$ ) for the full set of calculations performed. On the bottom part of the figure, where all results are collected together, one can see that all the points essentially follow a given line, depending only on the symmetry energy parametrization adopted. A larger equilibration (smaller  $R$ ) is observed in the *Asysoft* case, corresponding to the larger value of  $C_{sym}$ . We mention that, according to its definition, the imbalance ratio does not change if one considers as observable  $x$ , instead of the asymmetry of PLF and TLF, other observables linearly correlated to it and more accessible from the experimental point of view, such as isoscaling coefficients,

ratios of production of light isobars [29] or isotopic content of light particle emission [81].

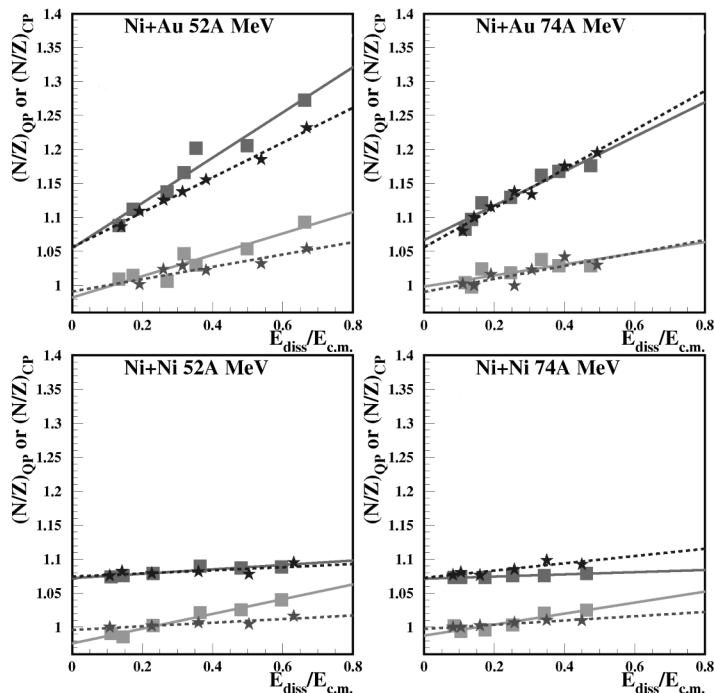


**Figure 9.** Isospin ratio of the quasi-projectile vs dissipated kinetic energy, for the two reactions and the two energies. For the stiff calculation, black stars and dotted lines display  $(N/Z)_{QP}$  and grey stars and dotted lines the  $(N/Z)_{CP}$  (BNV calculation followed by SIMON). Same conventions for the asy-soft case displayed by squares and full lines. The lines correspond to linear fits. Adapted from ref.[81].

*4.1.3. Comparison with Experimental Data* An experimental study of isospin diffusion as a function of the dissipated kinetic energy has been recently performed by the Indra collaboration [81].

Two systems, with the same projectile,  $^{58}\text{Ni}$ , and two different targets ( $^{58}\text{Ni}$  and  $^{197}\text{Au}$ ), at incident energies of 52 AMeV and 74 AMeV have been considered. This choice gives access to isospin effects in different conditions of charge (and mass) asymmetry, with respect to the analysis discussed in the previous sections, and to their evolution with the energy deposited into the system. In the symmetric Ni + Ni system isospin effects are essentially due to the pre-equilibrium emission. On the contrary, in the charge (and mass) asymmetric reactions, one can observe isospin transport between the two partners, leading to the neutron enrichment of the PLF. Hence, in the following, we will focus on the PLF properties. An isospin-dependent variable, correlated to the PLF asymmetry, is constructed from the isotopically identified particles emitted from the PLF:

$$(\langle N \rangle / \langle Z \rangle)_{CP} = \frac{\sum_{N_{ev}} \sum_{\nu} N_{\nu}}{\sum_{N_{ev}} \sum_{\nu} P_{\nu}}, \quad (11)$$

where  $N_\nu$  and  $P_\nu$  are respectively the numbers of neutrons and protons bound in the particle  $\nu$ ,  $\nu$  being d, t,  $^3\text{He}$ ,  $^4\text{He}$ ,  $^6\text{He}$ ,  $^6\text{Li}$ ,  $^7\text{Li}$ ,  $^8\text{Li}$ ,  $^9\text{Li}$ ,  $^7\text{Be}$ ,  $^9\text{Be}$ ,  $^{10}\text{Be}$ ; since neutrons are not measured free protons are excluded.  $N_{ev}$  is the number of events contained in a given bin of dissipated energy (or kinetic energy loss), that is used as a selector of the reaction centrality.

Simulations have been carried out considering two parametrizations of the symmetry energy: Asy-soft and Asy-stiff. Results are presented in Fig.9, that shows the evolution of the N/Z ratio of the PLF,  $N/Z_{QP}$ , as a function of  $E_{diss}/E_{c.m.}$ . One can see that N/Z increases with the centrality of the collision for the two systems and the two beam energies. For the Ni+Ni system the variation of N/Z with centrality is small, and attributed to pre-equilibrium emission. Indeed, for this system with a small neutron excess, more protons are emitted during the pre-equilibrium stage, especially in the asy-stiff case, due to the coupled effect of Coulomb repulsion and a less attractive symmetry potential for protons. This effect increases with the incident energy. On the contrary, the Asy-soft case tends to emit more preequilibrium neutrons leading to a lower N/Z ratio [1].

The evolution with centrality is much more pronounced for the neutron-rich and asymmetric Ni+Au system. In addition to pre-equilibrium effects, isospin transport takes place between the two partners of the collision, and increases with the violence of the collision, more for Asy-soft. It must be underlined that isospin equilibration is nearly reached, for the most central collision, at the lower energy for the Asy-soft EoS. However, when comparing diffusion effects corresponding to different Iso-EoS parametrizations, one should keep in mind that the isotopic content of the pre-equilibrium emission is also dependent on the Iso-EoS. In the Asysoft case, for instance, isospin diffusion is more effective but, at the same time, more neutrons are removed from the system by fast nucleon emission. In the mixed reaction, this reduces the sensitivity of the PLF asymmetry to the Iso-EoS. The same arguments hold for the comparison of results obtained at two different beam energies. In fact, pre-equilibrium emission is more abundant at higher energy. Isospin transport effects would be isolated by constructing imbalance ratios, as discussed before. However, such analysis is not possible for this set of data.

In figure 9 are also plotted the results concerning the variable  $(N/Z)_{CP}$ , calculated after de-exciting the hot primary PLF's with the help of the SIMON code [83]. The values of  $(N/Z)_{CP}$  are always smaller and the evolution with dissipation is generally flatter than that of the N/Z of the primary PLF: secondary decay weakens the isospin effects. However,  $(N/Z)_{CP}$ , which appears in the simulations to be linearly correlated with the N/Z of the primary PLF, is thus a good indicator of isospin transport effects and is sensitive to the Iso-EoS. Moreover, this observable can be directly compared to experimental data. This is shown in Fig.10. Open points show the values obtained forward in the nucleon-nucleon (NN) frame. In this case mid-rapidity particles and those coming from the PLF de-excitation are mixed up. Full points in Fig.10 are related to the values of  $(N/Z)_{CP}$  forward in the PLF frame. They are representative of the isotopic

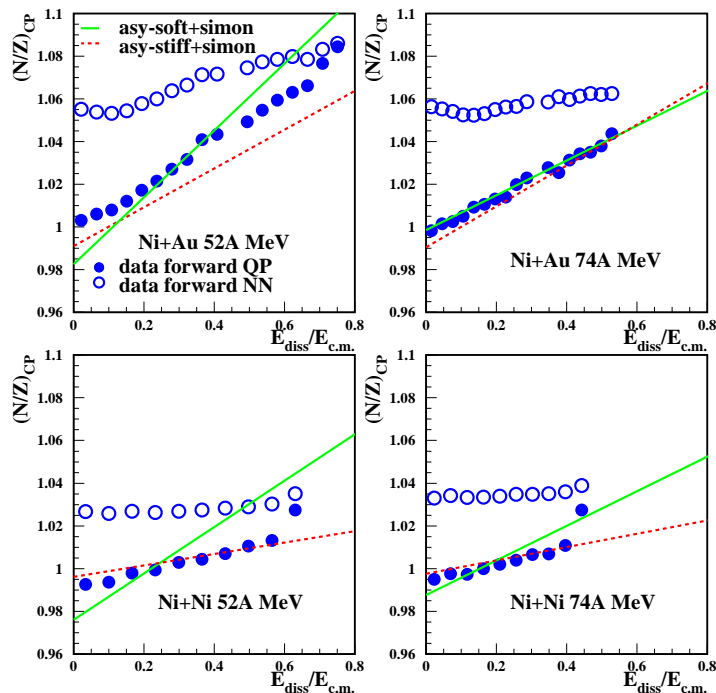


**Figure 10.** (color online) Isospin ratio of complex particles for Ni quasi-projectile vs dissipated kinetic energy, for the two reactions and the two energies. Circles correspond to the experimental data, open for data forward of the N-N velocity [82], full for data forward in the QP frame. Dotted lines and full lines as in fig. 9. Adapted from [81].

content of the particles emitted from the PLF only and can be compared with the results of the simulation, displayed in Fig.10 by the lines. When looking globally at the results for the four cases treated here, the agreement is better when the Asy-stiff EoS is used, i.e. a linear increase of the potential term of the symmetry energy around normal density. This is in reasonable agreement with the conclusion drawn from isospin diffusion in Sn+Sn systems at 50 A MeV, [84] see before, and matches the one derived from the competition between dissipative mechanisms for Ca+Ca, Ti at 25 A MeV [85].

#### 4.2. Isospin Distillation in Presence of a Radial Flow

The study of isospin effects in central collisions and, in particular, of the isospin distillation mechanism is interesting also in a more general context: in heavy ion collisions the dilute phase appears during the expansion of the interacting matter. Thus one can investigate effects of the coupling of expansion, fragmentation and distillation in a two-component (neutron-proton) system [88]. In the following we will discuss correlations between the isotopic content of IMF's and kinematical properties in central multifragmentation reactions. Fragmentation originates from the break-up of a composite source that expands with a given velocity field. Since neutrons and protons experience different forces, one may expect a different radial flow for the two species. Being these forces connected to the density dependence of the symmetry energy, one

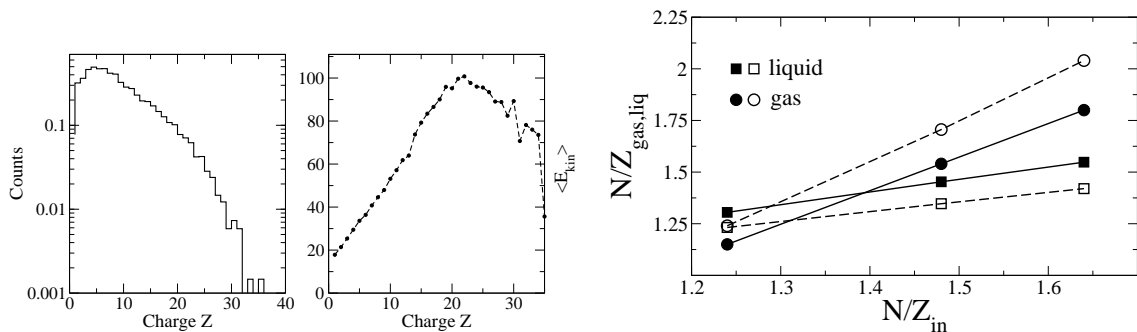


**Figure 11.** Left Panel: Fragment properties in the reaction  $^{112}\text{Sn} + ^{112}\text{Sn}$  at  $b = 2$  fm,  $E/A = 50$  MeV/nucleon,  $t = 300$  fm/c. Left: charge distribution. Right: average kinetic energies.

Right Panel: Asymmetry  $N/Z$  of the gas (circles) and of the liquid (squares) phase for central  $\text{Sn} + \text{Sn}$  collisions with different initial  $N/Z$ . Full lines and full symbols refer to the Asystiff, dashed lines and open symbols to the Asysoft parameterization.

should be able to extract information on its properties.

Such analysis is, in a way, complementary to the study of the isospin content of pre-equilibrium nucleon emission [72, 89], because it looks at the same phenomenon from the point of view of the fragmenting residual system. In fact, we will see that the behaviour is often the opposite of the one observed for the pre-equilibrium emission.

*4.2.1. Fragmentation Path in Central Collisions* We will focus on central collisions,  $b = 2$  fm, in symmetric reactions between systems having three different initial asymmetries:  $^{112}\text{Sn} + ^{112}\text{Sn}$ ,  $^{124}\text{Sn} + ^{124}\text{Sn}$ , and  $^{132}\text{Sn} + ^{132}\text{Sn}$  with  $(N/Z)_{in} = 1.24$ , 1.48 and 1.64, respectively. The considered beam energy is 50 MeV/nucleon. Calculations are carried out for two parameterizations of  $E_{sym}$ , Asysoft and Asystiff. The first two reactions,  $^{112}\text{Sn} + ^{112}\text{Sn}$  and  $^{124}\text{Sn} + ^{124}\text{Sn}$ , have been widely investigated both from the experimental and theoretical point of view [41, 90, 91, 92].

We first illustrate some general properties of the fragmentation mechanism in central events, as described by the SMF model. After the collisional shock and the initial compression, the composite nuclear source expands. Along this expansion, small density fluctuations are amplified by the unstable mean-field and large amplitude density gradients are developed. This process ends up with the formation of several fragments, corresponding to the high density bumps, located on a bubble-like configuration [33, 93]. Their average multiplicity is approximately equal to 6 for the reactions considered here [41]. Several nucleons are emitted, prior to fragmentation, at the early stage (pre-equilibrium emission) and/or are evaporated while fragments are formed. Primary fragments are identified by applying a coalescence procedure to the matter with density larger than  $\rho_{cut} = 1/5 \rho_0$  (that we classify as 'liquid phase'). The remaining nucleons are considered as belonging to the 'gas phase'.

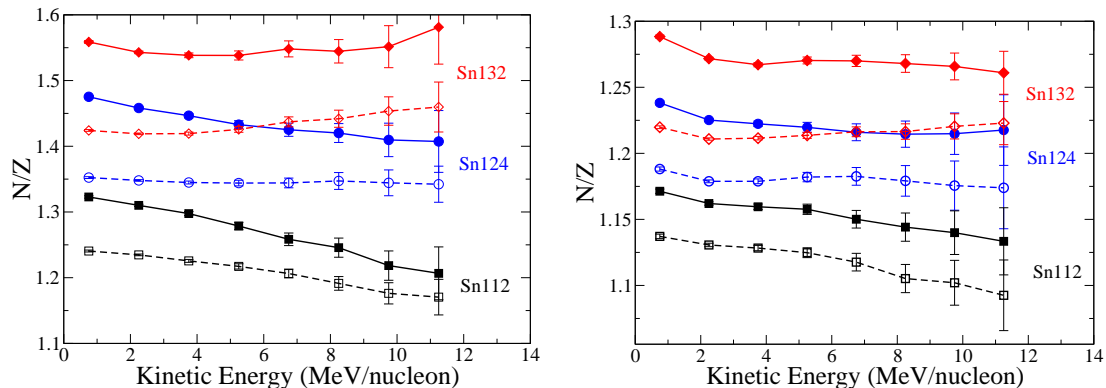


**Figure 12.** (color online) Left Panel. Fragment asymmetry  $N/Z$  (see text) as a function of the kinetic energy for different mass symmetric  $Sn + Sn$  collisions at  $b=2$  fm,  $E/A = 50$  MeV/nucleon. Solid lines are for the asystiff and dashed lines for the asysoft symmetry energy, and the different symbols distinguish the different collision systems.

Right Panel. Final fragment asymmetry  $N/Z$ , i.e. after evaporation, as a function of the kinetic energy (same format as in the Left Panel).

In Fig.11 (Left Panel) we show the fragment charge distribution (left) and the average kinetic energy as a function of the charge  $Z$  (right). From the linear increase of the kinetic energy with the fragment charge  $Z$  one can estimate the radial collective flow. The change of trend observed for big fragments reflects their different formation mechanism, via recombination effects or from PLF/TLF residues. We restrict our analysis to fragments with charge between 3 and 10 (IMF) produced in the fast break-up of the system; they represent the *liquid phase* with a clear evidence of radial flow.

The average  $N/Z$  of emitted nucleons (gas phase) and of the IMF's is presented in Fig.11 (Right Panel) as a function of the initial asymmetry,  $(N/Z)_{in}$ , of the three colliding  $Sn$  systems.

Generally, the gas phase is seen to be more neutron-rich while the IMF's are more symmetric. This is due to the combined action of the pre-equilibrium emission, that reduces the neutron excess of the composite system, and of the distillation mechanism acting in a later stage, while fragments are formed.

This trend is stronger in the Asysoft relative to the Asystiff case, since the symmetry energy is larger below saturation in the former case [41]. The difference between the asymmetries of the gas and liquid phases increases with the  $(N/Z)_{in}$  of the system, and is always larger in the Asysoft case. It should be noticed that the isotopic content of the gas phase appears more sensitive to the Iso-EoS than the asymmetry of the fragments. As one can see from Fig.11 (Right Panel), for the IMF's the difference between the two EoS's is just about 8%.

*4.2.2. Isospin-Velocity Correlations* Within a full detection of fragment properties, the investigation of the possible existence of correlations between size, isotopic and kinematical observables brings new information about the fragmentation mechanism, the expansion and cooling dynamics, and the nuclear interaction in the low density regime. For the range of charges considered in our analysis,  $3 < Z < 10$ , the average fragment size is loosely correlated to the velocity. In fact, as one can see from Fig.11 (Left Panel), small fragments have nearly the same collective velocity (kinetic energies proportional to the masses). Now we discuss more in detail the correlations between fragment isotopic content and kinematic properties. As a measure of the isotopic composition of the IMF's we will consider the sums of neutrons,  $N = \sum_i N_i$ , and protons,  $Z = \sum_i Z_i$ , of all IMF's in a given kinetic energy bin (here taken as 1.5 MeV/nucleon), in each event, taken at  $t = 300 fm/c$  (primary fragments). Then we take the ratio  $N/Z$  and consider the average over the ensemble of events. In Fig.12 (Left Panel) we report the dependence of this fragment asymmetry on the kinetic energy for the three reactions, and for the two parametrizations of the symmetry energy. The magnitude of the fragment asymmetry changes with the symmetry energy, as expected. Moreover the slopes of the curves in Fig. 12 (Left) appear particularly characteristic of the asymmetry of the initial system and of the stiffness of the symmetry energy. In fact, we expect two opposing trends since the Coulomb energy alone will accelerate the more proton-rich fragments. Thus the slope of the curve  $N/Z(E_{kin})$  will be negative, and more so for more proton-rich systems (e.g. in Fig.12(Left) the system  $^{112}Sn + ^{112}Sn$  has the largest negative slope). The symmetry energy, on the other hand, is more repulsive for more neutron-rich fragments, and thus the slope should be positive, more so for the softer symmetry energy (e.g. in Fig.12(Left) the slope for asysoft is always larger than for asystiff). When both forces are present there is a compensation between these two trends, and the final slope can be both negative or positive. It should increase for an Asysoft symmetry energy and neutron-richer systems. This is observed in Fig.12(Left) as a general trend.

*4.2.3. Secondary Decay Effects* So far we have discussed features related to primary fragments. However, in order to compare with experimental data, one cannot avoid treating the de-excitation process. For this we have calculated the excitation energy of the fragments in each event (which is found to be about  $2.5 \pm 1$  MeV/nucleon on the average), and used the statistical evaporation code SIMON [83] for the decay. The fragment  $N/Z$  ratios for the secondary fragments are shown in Fig.12(Right Panel) in the same format as in Fig.12(Left Panel) for the primary fragments. The final fragment  $N/Z$  ratio is found to be reduced by the secondary decay, due to the abundant neutron evaporation. It approximately follows the relation  $(N/Z)_{fin} \approx a(N/Z) + b$ , with  $a$  and  $b$  not much depending on the fragment kinetic energy and initial asymmetry ( $a \approx 0.55$  and  $b \approx 0.45$ ). It is also seen that a linear energy dependence is less well fulfilled than for the primary fragments, in particular for low kinetic energies. However, one can still appreciate the evolution of the  $N/Z$  energy dependence with the neutron richness of the initial systems and the difference between the predictions of the two iso-EOS's,

though the sensitivity is reduced with respect to primary fragments (compare Left and Right Panels in Fig.12 ). Finally we mention that, as far as the final fragment  $N/Z$  is concerned, results may depend on the evaporation code considered. This introduces an additional degree of uncertainty in the comparison to experimental data. The issue of a more accurate treatment of the de-excitation chain of neutron-rich nuclei should be critically addressed in the future.

### 4.3. Isospin Dynamics in Neck Fragmentation

*4.3.1. Experimental Survey* It is now quite well established that the largest part of the reaction cross section for dissipative collisions at Fermi energies goes through the *Neck Fragmentation* channel, with *IMFs* directly produced in the interacting zone in semiperipheral collisions on very short time scales [27, 28, 95]. We can predict interesting isospin transport effects for this new fragmentation mechanism since clusters are formed still in a dilute asymmetric matter but always in contact with the regions of the projectile-like and target-like remnants almost at normal densities. In presence of density gradients the isospin transport is mainly ruled by drift coefficients and so we expect a larger neutron flow to the neck clusters for a stiffer symmetry energy around saturation, [1, 96].

A systematic experimental study of midvelocity emission as a function of beam energy, violence of the collision and mass of the system has been performed in the last years by several groups [97, 98, 99, 100, 101], using different fragment multidetectors. They all agree on the evidence of two distinct sources of fragment production, one at mid-rapidity (the neck fragmentation) and one at the Quasi-Projectile rapidity (PLF\* evaporation) ( the detection velocity threshold was too high to clearly see the Quasi-Target emissions). All experiments also agree on a neutron enrichment of the mid-rapidity fragments, even in the cases of the same isospin asymmetry of the colliding ions, like  $Ni + Ni$  (almost charge symmetric) [99],  $^{64}Zn + ^{64}Zn$  [100],  $^{93}Nb + ^{93}Nb$  and  $^{116}Sn + ^{116}Sn$  [97, 98].

In the case  $^{114}Cd + ^{94}Mo$  at 50 AMeV [101] it was also shown that the fragments with charge  $3 \leq Z \leq 20$  at midrapidity exhibit a rather surprising similar neutron enrichment between central and midperipheral collisions. This could be an indication of an Asy-stiff behavior of the symmetry term below saturation which implies a reduced isospin distillation for fragments produced in central events via spinodal mechanism (see Sect.4.2) and a larger neutron flow to the neck region for semiperipheral collisions.

A very accurate analysis of neck fragmentation has been possible with the use of the CHIMERA Multidetector at Laboratori Nazionali del Sud-INFN, Catania, that for the very low threshold characteristic of the telescopes was allowing also a good detection of the emissions from the Target region. The reactions  $^{124}Sn + ^{64}Ni$  and  $^{112}Sn + ^{58}Ni$  at 35 AMeV were investigated in inverse kinematics [102, 103]. These conditions allowed an easy distinction between *IMFs* produced in the PLF, TLF and “neck” sources, allowing also important angular and velocity correlation measurements.

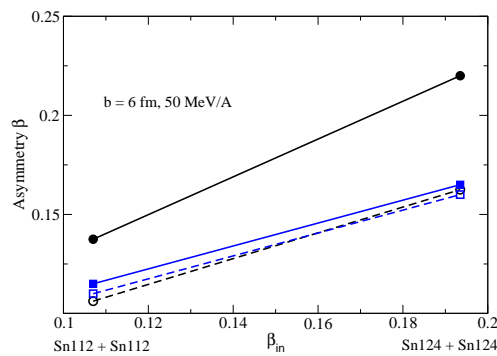


**Figure 13.** Ternary events in semiperipheral  $Sn + Sn$  collisions at 50  $AMeV$ . Asymmetry of IMF's (circles) and PLF-TLF (squares), as a function of the system initial asymmetry, for two Iso-EOS choices: Asystiff (full lines) and Asysoft (dashed lines).

A class of events was clearly identified for which the IMFs show deviations from velocity Viola systematics simultaneously with respect to PLF and TLF [104]. The angular distribution of those IMFs originating from the neck-like structure corresponds to a quite aligned configuration. The  $\Phi_{plane}$ , the angle between the fission axis (defined by the PLF-IMF system) projected in the reaction plane and scission axis (defined by PLF-TLF system) is centered around zero. Such alignment indicates that after the splitting of initial composite systems the ensemble PLF-IMF will rotate as a whole not for long period, resulting an early decoupling of the neck region from the two residues. The  $\Phi_{plane}$  distribution of heavier IMF's become wider while their velocities along beam axis suggest a continuous transition towards cases when they are more correlated with one of the two heavy residues and so emitted at later times without preferential alignment.

From such kinematic correlations it is possible, using Coulomb trajectory calculations, to calibrate a time-scale for fragment emission. These estimates lead to the conclusion that the lighter IMFs are produced between 40 fm/c to 80 fm/c from the reseparation while the heavier ones are formed even at 120 fm/c or longer. We can expect to see very different isospin content of the fragments in the different velocity and angular correlation bins: for IMFs with a given charge the greatest isospin value is acquired by those with the largest deviations from Viola systematics and the highest degree of alignment [108].

From these exclusive data we can extract important information on the  $Iso - EoS$  using microscopic *ab initio* transport approaches.

*4.3.2. Isospin Tracer of the Reaction Mechanism and Symmetry Energy* Several transport models were involved to explain various aspects of the reaction mechanisms and related isospin dynamics [105], [106], [107]. We employ Stochastic Mean Field transport simulations, see Sect.2, able to account for an accurate description of mean-field dynamics, very important at these energies, consistently coupled to dynamical fluctuations, essential to account for instabilities and fragment formation.

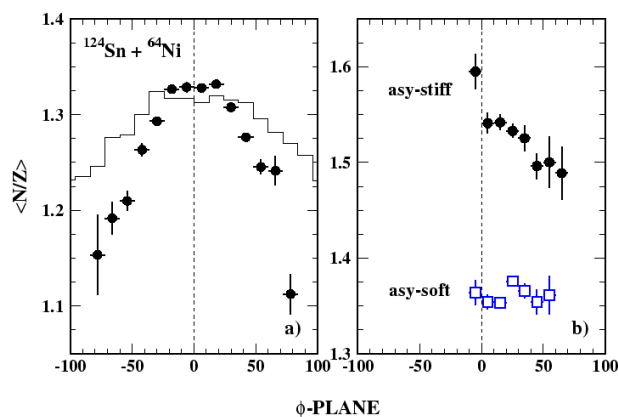


**Figure 14.** Correlation between  $N/Z$  of  $IMF$  and *alignment* in ternary events of the  $^{124}Sn + ^{64}Ni$  reaction at  $35 A MeV$ . *Left Panel.* Exp. results: points correspond to fast formed  $IMF$ s (Viola-violation selection); histogram for all  $IMF$ s at mid-rapidity (including statistical emissions). *Right Panel.* Simulation results: squares, Asysoft; circles, Asystiff.

The first point is to show the sensitivity to the density dependence of the symmetry term of the Isospin Migration from the PLF/TLF to the Neck region. We have analysed 200 SMF ternary events for semiperipheral  $^{112}Sn + ^{112}Sn$  and  $^{124}Sn + ^{124}Sn$  collisions at  $50 A MeV$ . In Fig.13 we present the correlation between the average asymmetry parameter  $\beta \equiv (N - Z)/A$  of the Fragments emitted at mid-rapidity and of the PLF/TLF residues vs the initial asymmetry of the colliding ions, using the stiff and soft density dependence of the symmetry term below saturation. As expected from the drift contribution (dominant here since the initial distribution of the asymmetry is uniform) proportional to the symmetry energy slope below saturation, we see a much larger neutron enrichment in the neck fragments for the Asystiff choice, Fig.3, more evident in the  $^{124}Sn$  n-rich case.

A very nice new analysis has been performed on ternary events in the  $Sn + Ni$  data at  $35 A MeV$  by the Chimera Collab.,[108], see Fig.14 left panel. For the mid-rapidity  $IMF$ s a strong correlation between neutron enrichment, alignment and Viola violation (when the short emission time selection is enforced) is seen, that can be reproduced only with a stiff behavior of the symmetry energy, Fig.14 right panel (for primary fragments) [109]. A more detailed study for each  $IMF$  Isotope clearly shows the same effect for the same kinematic selection bins [108]. All that represents a clear evidence in favor of a relatively large slope (symmetry pressure) around saturation. We note a recent confirmation from structure data, i.e. from monopole resonances in Sn-isotopes [110].

In conclusion we can figure out a continuous transition from fast produced fragments via spinodal and neck instabilities to clusters formed in a dynamical fission of the projectile(target) residues up to the evaporated ones (statistical fission). Along this line it would be even possible to disentangle the effects of volume and shape instabilities. From the previous discussion on the neutron enrichment of the overlap ("neck") region

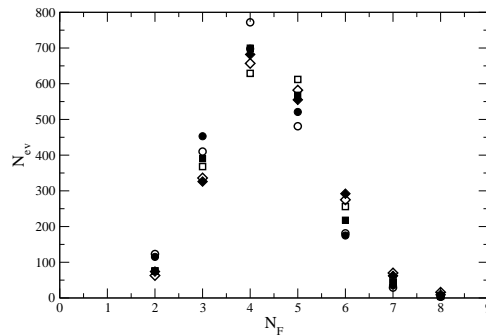


**Figure 15.** Fragment multiplicity distribution at  $b = 4 fm$ . Circles corresponds to LL, squares to HH while diamonds are associated with EE entrance channel combinations. Full symbols: Asysoft EoS. Open symbols: Asystiff EoS.

we can expect that the IMF Isospin content could be a good tracer of the Reaction Mechanism.

In the following we suggest new fragment mass-velocity-isospin correlations particularly sensitive to the various mechanisms as well as to the isovector part of the in-medium nuclear interaction. We remind that a study of just mass-velocity correlations for the fragmentation of quasiprojectiles was performed by Colin et al. [111] within the INDRA collaboration, revealing some evidence of break-up of very elongated structures.

*4.3.3. IMF Mass-Charge-Velocity Correlations* Here we focus on mass symmetric  $Sn+Sn$  reactions at 50 A MeV, intensively analyzed in the recent years at MSU [112]. We present a comparative study of the reactions  $^{132}Sn + ^{132}Sn$  (EE system),  $^{124}Sn + ^{124}Sn$  (HH) and  $^{112}Sn + ^{112}Sn$  (LL) at  $50 MeV/A$ . We shall focus on the value of impact parameter  $b = 4 fm$  where some memory of the entrance channel, through the existence of well defined PLF and TLF like fragments, together with a quite large multiplicity of intermediate mass fragments, is observed [41]. A total number of 2000 events is generated for each case and for the two iso-EoS considered. In Figure 15 we report the IMF multiplicity distribution for all reactions. We observe that the SMF model is able to reproduce the general feature that a more neutron rich combination enhances the IMF's multiplicity.

To get a deeper insight into the nature of the fragmentation process, we adopt an analysis of kinematical properties which was previously employed in studies concerning dynamical fission or neck fragmentation mechanisms [113, 114].

The asymptotic velocities of PLF and TLF-like residues define an intrinsic axis of the event by the vector  $\mathbf{V}_r = \mathbf{V}(H_1) - \mathbf{V}(H_2)$ , always oriented from the second heaviest fragment  $H_2$  towards the heaviest one  $H_1$ . The intermediate mass fragments of each event are ordered in mass and the orthogonal and parallel components of their asymptotic velocities, with respect to the intrinsic axis, are determined.

In Figure 16 the charge distributions corresponding to each order in hierarchy are shown for the events with three IMFs and all entrance channel combinations, HH, EE

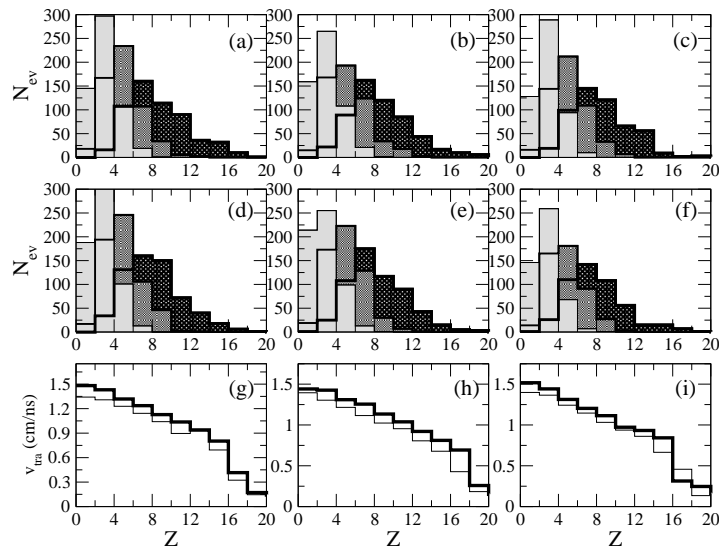


**Figure 16.** Charge distribution of each IMF of the hierarchy for Asysoft EoS (upper row) and Asystiff EoS (middle row). HH combination: (a),(d),(g). EE combination: (b),(e),(h). LL combination: (c),(f),(i). Average transverse velocity distribution as a function of charge (bottom row) for Asysoft EoS (thick line) and Asystiff EoS (thin line). All results refer to events with IMF multiplicity equal to three. The shading of the distributions brightens according to the rank of the fragment in hierarchy.

and LL respectively. In all figures the histograms brighten as the rank of the IMF increases. The heaviest IMF (the rank one in hierarchy) can have a charge up to  $Z = 16 - 18$  and the distribution is centered around  $Z = 6 - 8$  while the lightest extends up to  $Z = 8$ . The average transverse velocity in each charge bin was calculated considering the contribution of all fragments, independently of the position in hierarchy (see Figure 16 (g), (h) and (i)). One observes a step decreasing trend with the charge, in agreement with previous findings reported in [115]. Since similar results are obtained for all entrance channel combinations we discuss in the following only the case of the HH system. In Figure 17 we report the IMF transverse and parallel velocity distributions for Asysoft EoS. We also plot the parallel velocity distributions of projectile and target like residues. In agreement with our definition for the intrinsic axis of the event, the velocity of the heaviest residue is always the positive one.

The transverse velocity distribution shifts towards higher values with the position in the mass hierarchy, the lightest fragment acquiring higher velocities. The same behavior is observed for the class of events with four IMF's and also for Asystiff EoS. This hierarchy in the velocity perpendicular to the intrinsic axis emerges as a specific signal characterizing the transition from multifragmentation to neck fragmentation. It can be related to the peculiar geometrical configuration of the overlapping region and to its time evolution. Due to the Coulomb repulsion, neck fragments are essentially emitted on the transverse plane. At variance light fragments, formed in a fast spinodal mechanism, have shorter emission time and acquire larger transverse velocity. It is interesting to

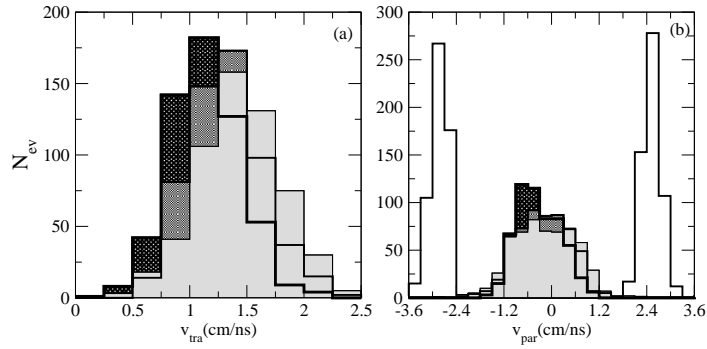


**Figure 17.** (a): Transverse velocity,  $v_{tra}$ , distributions for fragmentation events with three IMF's. (b): Parallel velocity distribution for fragmentation events with three IMF's. Asysoft EoS and HH combination. The lightest shading corresponds to the lightest fragment in the event.

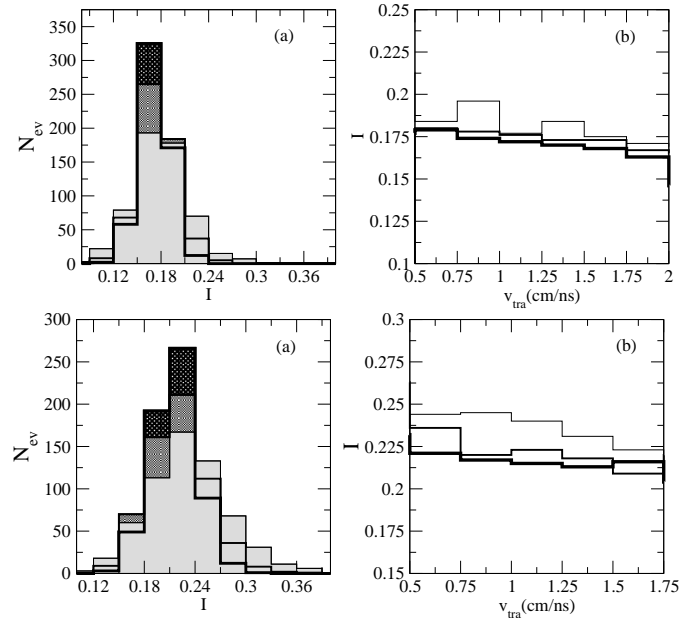


**Figure 18.** Asymmetry distribution of each fragment in hierarchy for fragmentation events with three IMF's (a). Average asymmetry of each IMF in hierarchy as a function of transverse velocity for events with three IMF's (b). Upper Panel: Asysoft EoS and HH combination. Bottom Panel: Asystiff and HH combination

notice that similar features are observed in central reactions (see previous Section), but with respect to the collective radial velocity.

The features discussed above are determined mainly by the isoscalar part of the equation of state, on top of which the symmetry energy may induce minor changes. This explains the tiny difference between the two Iso-EoS. On the other hand, the properties related to the fragment isotopic content are directly influenced by the symmetry energy term. We have extended our investigation to this observable studying its dependence on the IMF position in hierarchy, as well its correlation to transverse velocity, similarly

to the analysis done for central collisions (see previous Section). In Fig.18(a), Upper Panel for Asysoft EoS and Bottom Panel for Asystiff EoS, we report the asymmetry  $I = (N - Z)/(N + Z)$  distribution of each IMF of the hierarchy. The results refers to HH system whose initial asymmetry is  $I = 0.194$ .

For Asysoft EoS the isospin distributions are centered at lower values and have rather narrow widths, quite insensitive to the position in hierarchy. At variance, for Asystiff EoS the centroids of the distributions are closer to the initial value of the composite system and their broader widths depend on the rank in the mass hierarchy. For both equations of state the lightest IMFs are more likely to acquire higher values of asymmetry pointing towards different production mechanisms or formation conditions.

We relate these features to the differences between the behavior of the two Iso-EoS at subsaturation densities. Clearly, larger values of the symmetry energy (Asysoft case) fasten the isospin distillation process and all IMF's reach closer isospin values. On the other hand, for Asystiff EoS fragments grow in low density, more charge asymmetric domains, as a result of isospin migration towards the neck. The differences inside the hierarchy in this case point towards different formation time scales with the lightest IMF finding a neutron rich environment, being the distillation process not efficient enough to lower the isotopic content of all IMF's in the event. If they have lower transverse velocity, remaining longer in a neutron-richer region, they will carry higher asymmetry. The average fragment asymmetry, as a function of the transverse velocity, is shown in Fig.18 (b), Upper Asysoft and Bottom Asystiff EoS. A decreasing trend is manifest for all IMF's, more pronounced for the latter choice. In this case, for a given transverse velocity bin the asymmetry always increases with the rank in hierarchy.

These observations open new opportunities also from the experimental point of view. An analysis of isospin dependent observables in correlation to the position in mass hierarchy or kinematic observables can add new constrains on the behavior of the symmetry energy below normal density and provide indications about the formation of IMFs in the low density and heated overlapping region at these impact parameters. Recent experimental results reported by the CHIMERA collaboration for the system  $Sn + Ni$  at a lower energy ( $35A MeV$ ) [116] suggest the existence of the hierarchy in transverse velocity, as discussed here. In these experiments it was also found that the lightest fragments are more asymmetric. This sensitivity to the rank in the hierarchy can then be related to a asystiff-like behavior of the symmetry energy at sub-saturation densities.

## 5. Isospin Effects at High Baryon Density: Effective Mass Splitting and Collective Flows

At higher energies, where suprasaturation densities will be probed, all the observables under investigation are more affected by the Momentum Dependence (MD) of the mean fields. This represents a further obstacle for the determination of  $E_{sym}$  at high  $\rho$ , even because the MD has also an isoscalar contribution that is influencing the reaction

dynamics, as shown in the previous Section. However, the possibility to have access experimentally to several observables as a function of momentum in a wide range offers the real possibility to disentangle density and momentum dependence of the symmetry potentials ( $n/p$  effective masses). Generally, all Relativistic Mean Field (RMFT) approaches give  $m_n^* < m_p^*$  in neutron-rich matter, while in non-relativistic models generally  $m_n^* > m_p^*$  with some exceptions [43, 42]. Non-relativistic Brueckner-Hartree-Fock (BHF) [117] would indicate the last choice as the correct one, which means that the Lane Potential  $U_{Lane} \equiv (U_p - U_n)/2\beta$ , with  $\beta$  asymmetry parameter, decreases with  $k$ . In RMFT one finds the opposite trend but it lacks the effect of the finite range of the interaction. In Dirac-BHF both relativistic fields and the finite range effect are included, but there exists an ambiguity from the method used to project on the different Lorentz amplitudes [2, 4]. One could judge that the microscopic approaches favour the relation  $m_n^* > m_p^*$ , but in any case it is mandatory to show that this is the case in HIC by means of a comparison with the available and forthcoming data.

Our Stochastic Mean Field (*SMF*) transport code has been implemented with *Iso - MD* symmetry potentials, with a different  $(n, p)$  momentum dependence, as discussed in detail in Sect.2. This will allow to follow the dynamical effect of opposite  $n/p$  effective mass splitting while keeping the same density dependence of the symmetry energy [46, 52].

We present here some results for  $^{197}\text{Au} + ^{197}\text{Au}$  reactions at  $400\text{AMeV}$  [52]. For central collisions in the interacting zone we can reach baryon densities about  $1.7 - 1.8\rho_0$  in a transient time of the order of 15-20 fm/c. The system is quickly expanding and the Freeze-Out time is around 50fm/c. At this time we have a dominant Coulomb interaction among the reaction products. All the results presented here refer to this time step. Secondary decays of excited primary fragments are not accounted for. In fact this will not affect too much the properties of nucleons and light ions at high transverse momenta mostly discussed in this work.

### 5.1. Isospin Ratios of Fast Emitted Particles

In Fig.19 we plot the  $(n/p)$  and  $^3\text{H}/^3\text{He}$  yield ratios at freeze-out, for two choices of Asy-stiffness and Mass-splitting, vs. transverse momentum in a mid-rapidity selection (upper curves) and kinetic energy (all rapidities, lower curves). In this way we can separate particle emissions from sources at different densities, as discussed in Sect 2.

We clearly observe the opposite effect of the different mass splitting in the low and high momentum regions, as expected from Fig.4. E.g. in the  $m_n^* < m_p^*$  case the neutrons see a less repulsive potential at low momenta and a more repulsive one at high  $p_t$ . The curves in the opposite mass-splitting show exactly the opposite behavior. We note some interesting features:

i) The effect is almost not dependent on the stiffness of the symmetry term. At high  $p_t$ , where particles mostly come from high density regions, the larger repulsion seen by neutrons in the Asy-stiff case, leading to an enhanced emission, is compensated by the

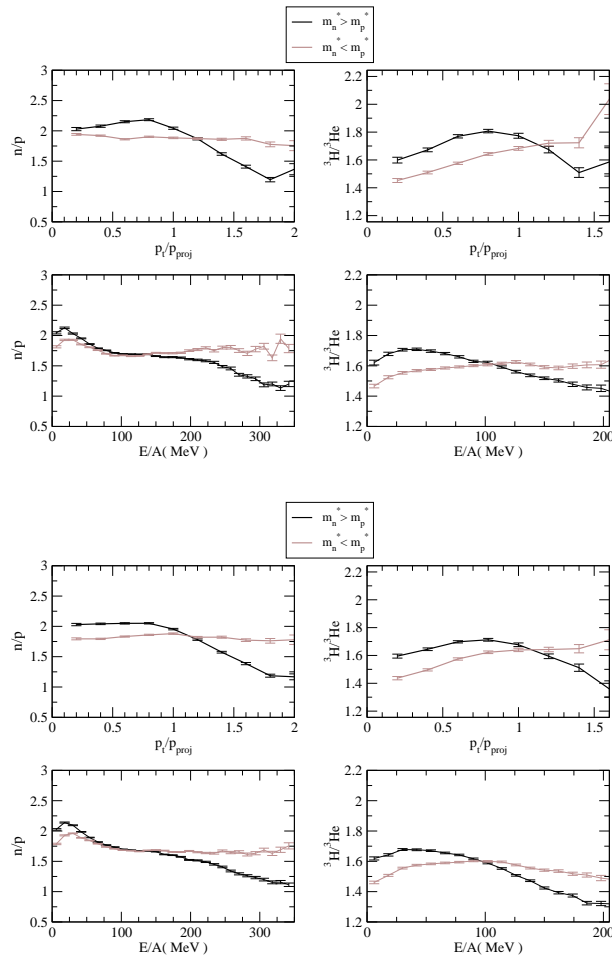


**Figure 19.**  $197\text{Au}+197\text{Au}$  at  $400\text{A MeV}$ , central collision. Isospin content of nucleon (left) and light ion (right) emissions vs.  $p_t$  at midrapidity,  $|y_0| < 0.3$ , (upper) and kinetic energy (lower), for all rapidities, for the two nucleon mass splitting choices. Top Panels: Asysoft; Bottom Panels: Asystiff.

larger Coulomb repulsion in the remaining matter, favoring proton emission. On the other hand, at low  $p_t$ , the sensitivity to the Asy-stiffness is lost due to the mixing of sources at different densities, also for central rapidities, during the radial expansion.

ii) The curves are crossing at  $p_t \simeq p_{projectile} = 2.13 fm^{-1}$ . The crossing nicely corresponds to the Fermi momentum of a source at baryon density  $\rho \simeq 1.6\rho_0$ , [43, 45, 46].

We remark that all the effects discussed before should be also present for the  ${}^3H/{}^3He$  yield ratios, more easily detected. Particularly interesting is the predicted large increase at high  $p_t$  in the  $m_n^* < m_p^*$  choice. Some preliminary FOPI results seem to indicate this trend [118], but more data are needed. It is encouraging that we already see a good  $Iso - MD$  dependence of rather inclusive nucleon/cluster emission data. In presence of a good statistics for the detection of high  $p_t$  particles, a further selection at high azimuthal angles and central rapidities would certainly enhance the sensitivity to the momentum dependence of the Symmetry Potentials. This will introduce the discussion of isospin elliptic flows of the following Subsection.

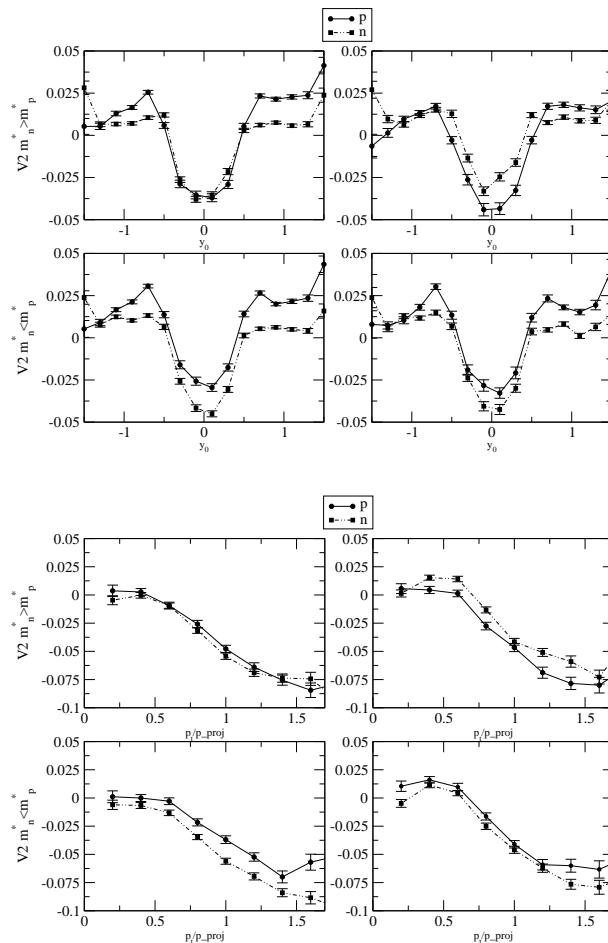


**Figure 20.** Proton (thick) and neutron (thin)  $V_2$  flows in a semi-central reaction Au+Au at 400AMeV. Top Panels: Rapidity dependence. Bottom Panels: Transverse momentum dependence at midrapidity,  $|y_0| < 0.3$ . Upper curves for  $m_n^* > m_p^*$ , lower curves for the opposite splitting  $m_n^* < m_p^*$ . Left: Asystiff. Right: Asysoft.

## 5.2. Isospin Flows

Isospin effects on collective flows have been studied within the *UrQMD* transport model in order to probe the influence of the symmetry repulsion at high densities [120, 121], here we focus the attention on the mass-splitting contributions. For the same Au+Au reactions, in a semicentral selection, we present in Fig. 20 (Top Panels) the rapidity dependence of  $(n/p)$  elliptic flow  $V_2$  for different choices of the Asy-stiffness and effective mass splitting. We observe the relevance of the latter: at mid-rapidity the neutron squeeze-out is much larger in the  $m_n^* < m_p^*$  case independently of the stiffness of the symmetry term. We note however that in the Asysoft case we see an inversion of the neutron/proton squeeze-out at mid-rapidity for the two effective mass-splittings. Good data seem to be suitable to disentangle *Iso* – *MD* potentials.

The mass-splitting effect is large at high  $p_t$  (Bottom Panels), again in a mid-rapidity selection, as expected for particle emitted from higher density regions. Here the results are also slightly depending on the Asy-stiffness, with large neutron *squeeze-out* effects

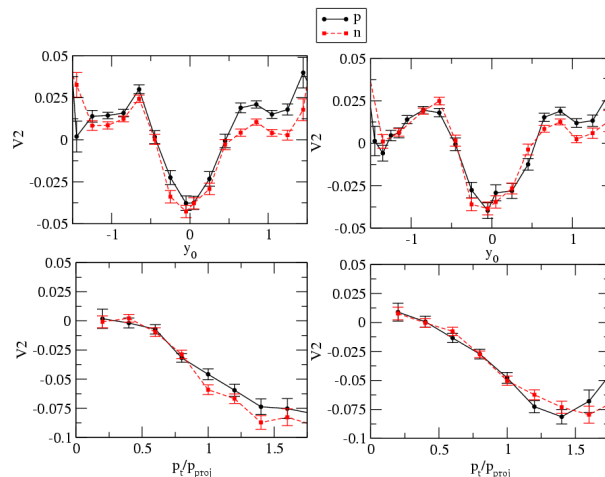


**Figure 21.** (color online) Proton (thick) and neutron (thin)  $V_2$  flows in a semi-central reaction Au+Au at 400 A MeV, for equal (n,p)-effective masses. Top Panels: Rapidity dependence. Bottom Panels: Transverse momentum dependence at midrapidity. Left: Asystiff. Right: Asysoft.

in the Asystiff case.

In order to have a clear idea of the relevance of the (n,p) mass splitting on the fast nucleon emissions we present in Fig.21 the neutron/proton elliptic flows for semicentral Au+Au collisions at 400 A MeV evaluated with the parametrizations giving  $m_n^* = m_p^*$  for the  $^{197}\text{Au}$  asymmetry  $\beta \simeq 0.2$ . Now the isospin effects are only related to the different stiffness of the symmetry term at suprasaturation density. We see that, at variance with the mass-splitting results of Fig.20, the rapidity distributions (top panels) are not much affected, with a slightly larger neutron squeeze-out in the Asystiff case. Consistently we see some difference in the transverse momentum dependence at mid-rapidity (bottom panels) only at very large  $p_t$ .

Due to the difficulties in measuring neutrons, we have analyzed the isospin sensitivity of light isobar flows, like  $^3\text{H}$  vs.  $^3\text{He}$  and so on. We still see effective mass splitting effects, although slightly reduced. As in the nucleon elliptic flow, at mid-rapidity the triton squeeze-out is larger in the  $m_n^* < m_p^*$  case independently of the stiffness of the symmetry term. Again in the Asysoft case we see an inversion of the  $^3\text{H}$  vs.  $^3\text{He}$  squeeze-out at mid-rapidity for the two choices of the mass-splitting. Some larger mass-splitting effects can be seen at high  $p_t$ . This should be well observed in the flow difference, with a good statistics.

We would expect the *Iso* – *MD* effects to increase with beam energy, due to the larger momenta of the emitted particles and to the reached higher densities in the compression stage. In this respect an interesting positive result is coming from preliminary FOPI data on  $^3\text{H}$  vs.  $^3\text{He}$  flows, for Au-Au collisions at beam energies extended up to 1.5 A GeV. The triton  $V_2$  shows a larger squeeze-out at mid-rapidity (in a relatively high transverse momentum selection) [118]. New more accurate and exclusive data will soon appear. We like to mention the new measurements that will be performed

at SIS-GSI by the ASYEOS Collaboration [122] and the new experiments planned at RIKEN-Tokyo and CSR-Lanzhou also with unstable, more neutron-rich, beams.

## 6. The Relativistic Structure of $E_{sym}$

The determination of  $E_{sym}$  at high density  $\rho > 1.5\rho_0$  needs to exploit HIC's at beam energies of  $E/A \geq 400\text{MeV}$  in order that the maximum density is sufficiently high. For the theoretical approaches this shifts the energy regime of interest to a range where relativistic effects can start to become significant. Hence relativistic, covariant approaches should be preferred; nonetheless relativistic extensions of non-relativistic approaches represent a viable way even if they may mix relativity and many-body effects[13]. In this section we briefly recall the relativistic structure of  $E_{sym}$  in effective hadronic models based on nucleons interacting through mesonic fields. At the level presented here the structure of  $E_{sym}$  is shared by the different models based on effective Lagrangians of Quantum-Hadro-Dynamics (QHD) [123], as the Relativistic Mean Field Theory (RMFT) [1, 34, 124], the Density Dependent Relativistic Hartree approach (DDRH)[125], the Effective Field Theory (EFT) density functional[126] as well as the microscopic Dirac-Brueckner-Hartree-Fock (DBHF) [127, 128]. Therefore the following discussion allows to set a common language that will be useful in the discussion about the meson production and the transition to quark matter of the next two Sections.

In QHD the effect of nuclear interactions results in in-medium modifications of the scalar effective masses and the energy-momentum four-vector

$$m_{n,p}^* = m + \Sigma_\sigma \pm \Sigma_\delta, \quad k_{n,p}^{\mu} = k^\mu + \Sigma_\omega^\mu \pm \Sigma_\rho^\mu, \quad (12)$$

where the different self-energies  $\Sigma_i$  are labelled by the mesons representative of the specific spin-isospin quantum numbers of field (isoscalar, Lorentz scalar/vector,  $\sigma/\omega$  and isovector, scalar/vector,  $\delta/\rho$  fields). The upper and lower signs refer to neutrons and protons, respectively. In neutron-rich asymmetric matter we systematically derive a  $m_n^* < m_p^*$  condition, even in the non-relativistic limit [1, 43]. The isovector self-energies can be written as

$$\Sigma_\delta(n, p) = -f_\delta \rho_{s3}, \quad \Sigma_\rho^\mu(n, p) = f_\rho j_3^\mu, \quad (13)$$

where  $\rho_{s3} = \rho_{sn} - \rho_{sp}$  and  $j_3^\mu = j_n^\mu - j_p^\mu$  are the scalar isospin density and the isospin current, respectively. In the most simple models of RMFT the coupling vertices  $f_i$  are constant, while in more sophisticated models. as e.g. the DDHF, they are density and even momentum dependent [129].

The symmetry energy arising from such a structure can be written as [1, 34]

$$E_{sym} = \frac{1}{6} \frac{k_F^2}{E_F^*} + \frac{1}{2} \left[ f_\rho - f_\delta \left( \frac{m^*}{E_F^*} \right)^2 \right] \rho_B \simeq \frac{1}{6} \frac{k_F^2}{E_F^*} + \Sigma_\rho^0 + \frac{m^*}{E_F^*} \Sigma_\delta \quad (14)$$

with  $E^* \equiv \sqrt{k^2 + m^*}$ , where  $f_\rho, f_\delta$  are the couplings of the nucleons to the effective isovector scalar and vector field. However already from the Hartree-Fock theory as well as from the more complete DBHF approach it is clear that each spin-isospin channel

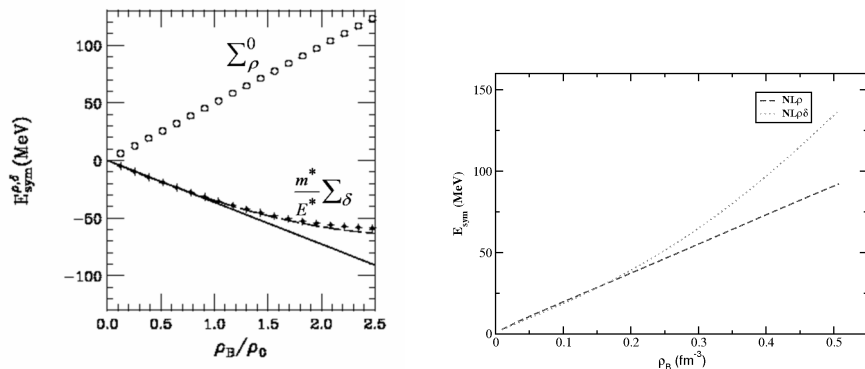


**Figure 22.** Left Panel: density dependence of scalar and vector isovector self-energies in NL-RMFT; the solid line is to highlight the deviation from linearity. Right Panel: corresponding symmetry term with and without the  $\delta$  contribution.

receives contributions from all the meson-like fields and the meson label is only indicative of the channel [130]. Eq.(14) can be strictly derived only in RMFT, but for our purpose the key point is that  $E_{sym}$  arises from a competition of two fields, one scalar and one vector, that at  $\rho \sim 2\rho_0$  are of the order of  $\sim 100$  MeV, as is shown in Fig.22 (Left panel) for a standard non-linear (NL)-RMFT model [131]. Since the attractive  $\delta$ -contribution is proportional to the scalar density, reduced by a factor  $m^*/E_F^*$  respect to the baryon density, the net effect will be a faster increase of the potential part of the symmetry energy at high densities [1, 34], as shown in the right panel of Fig.22. This behaviour is shared by all relativistic approaches, with the difference that for example in DDRH the coupling  $f_{\rho,\delta}$  depends on density, similarly in DBHF [132].

We stress the distinction between a scalar and a vector field because their balance in equilibrium conditions is generally dynamically broken for an evolving system. In Ref.[13] it has been shown that such an effect simulates a stiffer symmetry energy in the build-up of collective flows. In fact, the difference of the force acting on a neutron and a proton moving with momentum  $\vec{p}$  can be written, after some approximations, as

$$\frac{d\vec{p}_p}{d\tau} - \frac{d\vec{p}_n}{d\tau} \simeq 2 \left[ \gamma f_\rho - \frac{f_\delta}{\gamma} \right] \vec{\nabla} \rho_3 > \frac{4}{\rho_B} E_{sym}^{pot} \vec{\nabla} \rho_3, \quad (15)$$

where  $\gamma$  is the Lorentz factor  $E^*/m^*$ . We can see that dynamically the vector field is enhanced and the scalar field suppressed resulting in an effective  $E_{sym}^*$  larger than  $E_{sym}^{pot}$  as can be seen by comparing Eqs.(14) and (15). Hence, the relativistic structure implies a modified relation between  $E_{sym}$  and observables in HIC's. Of course, one can simulate this relativistic structure with the help of a specific momentum dependence, but this entangles many-body effects with relativistic ones. A first analysis has shown that such effects are significant for  $E/A > 1$  GeV [13].

## 7. Isospin Effects on Meson Production in Relativistic Heavy Ion Collisions

The phenomenology of isospin effects on heavy ion reactions at intermediate energies (few  $A\text{GeV}$  range) is extremely rich and the meson production can allow a “direct” study of the Lorentz structure of the isovector interaction in a high density hadron medium. We work within a relativistic transport frame, beyond the cascade picture, consistently derived from effective Lagrangians, where isospin effects are accounted for in the mean field and collision terms. We show that rather sensitive observables are provided by the pion/kaon production ( $\pi^-/\pi^+$ ,  $K^0/K^+$  yields). Relevant non-equilibrium effects are stressed.

In this energy range lower mass mesonic states, namely pions and kaons, can be excited. Therefore symmetry energy effects are transferred to the production of mesons. In Ref.[135] it was suggested that the  $\pi^-/\pi^+$  ratio is sensitive to  $E_{sym}(\rho)$ . It was claimed that the main effect consists in the emission of nucleons during the evolution depending on  $E_{sym}$  leading to a different  $n/p$  content of the residual system, which in turn influences the formation of the different charge states of the pion.

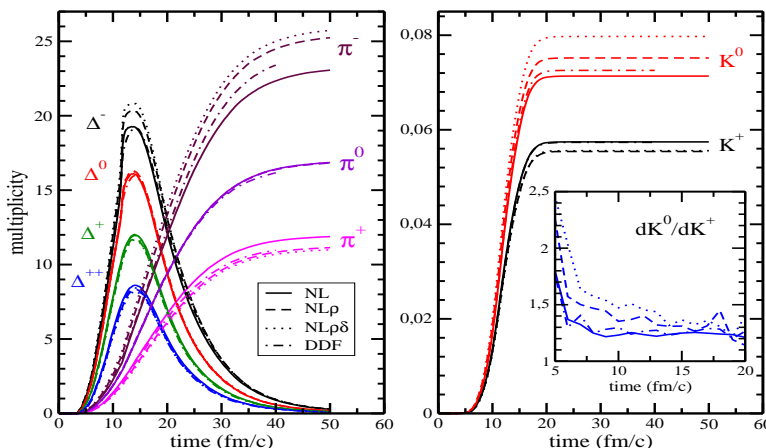


**Figure 23.** (color online) Time evolution of the  $\Delta^{\pm,0,++}$  resonances and pions  $\pi^{\pm,0}$  (left), and of kaons ( $K^{\pm,0}$ ) (right) for a central ( $b = 0$  fm impact parameter) Au+Au collision at 1 AGeV incident energy. Transport calculation using the  $NL$ ,  $NL\rho$ ,  $NL\rho\delta$  and  $DDF$  models for the iso-vector part of the nuclear  $EoS$  are shown. The inset shows the differential  $K^0/K^+$  ratio as a function of the kaon emission time.

Even if this mechanism seems quite straightforward one may doubt its real effectiveness. Indeed, the idea of using pions to determine the symmetric part of the EoS has suffered from the fact that pions strongly interact with nucleons and are produced during the whole evolution of the collision system making it difficult to associate their production to a specific density reached during the collision. In that context it was suggested by Aichelin and Ko [136] that kaons are a better probe of the EoS. The reason is twofold. Kaons have a higher threshold energy, hence they are produced only in the high density phase. Moreover, once produced they interact weakly with nucleons and their width with respect to the mass is quite small making a quasi-particle approximation

more reliable. After nearly 20 years the effort to determine the symmetric EoS by kaon production has been successful and is summarized in Ref.[137]. Following the same line of thinking the Catania group has suggested to investigate the  $K^0/K^+$  ratio as a better probe of the  $E_{sym}$  at high density [15, 16, 109] (the other isospin pair with anti-kaons  $\bar{K}_0/\bar{K}^-$  suffers from the strong coupling to the medium).

Using a relativistic transport approach (Relativistic Boltzmann-Ühling-Uhlenbeck, RBUU [138]) we have analyzed pion and kaon production in central  $^{197}\text{Au} + ^{197}\text{Au}$  collisions in the  $0.8 - 1.8 \text{ AGeV}$  beam energy range, comparing models with the same “soft” EoS for symmetric matter and with different effective field choices for  $E_{sym}$ . Fig.23 reports the temporal evolution of  $\Delta^{\pm,0,+}$  resonances, pions ( $\pi^{\pm,0}$ ) and kaons ( $K^{+,0}$ ) for central Au+Au collisions at  $1 \text{ AGeV}$  [16, 139, 140] It is clear that, while the pion yield freezes out at times of the order of  $50 \text{ fm}/c$ , i.e. at the final stage of the reaction (and at low densities), kaon production occurs within the very early (compression) stage, and the yield saturates at around  $15 \text{ fm}/c$ , when the nucleon and  $\Delta$ 's densities reach their maximum value. From Fig.23 we see that the pion multiplicities are moderately dependent on the isospin part of the nuclear mean field. However, a slight increase (decrease) in the  $\pi^-$  ( $\pi^+$ ) multiplicity is observed when going from a NL-RMFT model without isovector fields (NL) to one with a  $\rho$  meson ( $NL\rho$ ) and with  $\rho$  and  $\delta$  mesons ( $NL\rho\delta$ ). This trend is more pronounced for kaons, see the right panel, due to the high density selection of the source and the proximity to the production threshold. Moreover isospin effects enter twice in the two-step production of kaons, see [15, 16].

In Fig.24(left) the pion and kaon ratios from these calculations are shown as a function of beam energy. The ratios decrease with beam energy, because the relative effects of mean fields and thresholds become less important. However, the greater sensitivity of the kaon ratios is seen clearly, since kaons emerge from high density regions (see the inset in the right panel of Fig.23. In this respect transverse momentum selections of the  $\pi^{-,+}$  yields would be very useful.

We have to note that in a previous study of kaon production in excited nuclear matter the dependence of the  $K^0/K^+$  yield ratio on the effective isovector interaction appears to be much larger (see Fig.8 of ref.[15]). The point is that in the non-equilibrium case of a heavy ion collision the asymmetry of the source where kaons are produced is in fact reduced by the  $n \rightarrow p$  “transformation”, due to the favored  $nn \rightarrow p\Delta^-$  processes. This effect is almost absent at equilibrium due to the inverse transitions, see Fig.3 of ref.[15]. Moreover in infinite nuclear matter even the fast neutron emission is not present. This result clearly shows that chemical equilibrium models can lead to uncorrect results when used for transient states of an *open* system.

At present there are essentially no data for kaons, while there are some for pions and  $\pi^-/\pi^+$  ratios from FOPI collaboration [141]. Within an isospin and momentum dependent transport model it has been claimed that an agreement with data can be achieved only if a very soft  $E_{sym}(\rho)$  is employed [142]. Such a finding appears in strong disagreement with other studies that exploit the elliptic flow to extract the slope of  $E_{sym}$  around and above the saturation density [143]. Moreover a recent transport evaluation

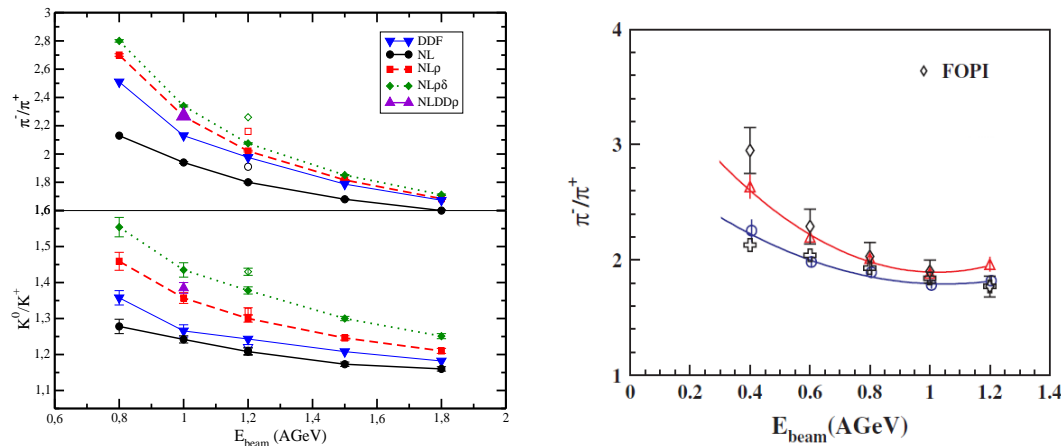


**Figure 24.** (color online) Left: Excitation function of the  $\pi^-/\pi^+$  and  $K^0/K^+$  ratios for  $Au + Au$ . RBUU results for different behavior of  $E_{\text{sym}}(\rho)$  [16]. Right: Results for  $Au + Au$  in IBUU04 for a soft (triangles) and a stiff (circles)  $E_{\text{sym}}$  [142] compared to the data from FOPI (diamonds) and a calculation with IQMD (crosses). Adapted from [142].

of the  $\pi$  ratio, also in a non-relativistic frame, is reaching just opposite conclusions [144].

The effect described in Ref.[142] essentially is due to the fact that a stiff  $E_{\text{sym}}$  causes a neutron-rich emission of nucleons in the early stages of the reaction leaving the system too symmetric in isospin content to reproduce the  $\pi^-/\pi^+$  ratio of FOPI. On the other hand, if one employs an  $E_{\text{sym}}(\rho)$  that just above  $\rho_0$  decreases with density generating an isospin force that is attractive for the neutrons it is possible to get close to the data, see Fig.24 (right). However, we note that it is mandatory to check if one can reproduce at the same time the  $n/p$  emission as a function of  $p_t$  especially at the high  $p_t$  relevant for pion production, since this represents the complementary signal for the soft  $E_{\text{sym}}$ , see Sect.5. This would be a first test of the claim for a very soft  $E_{\text{sym}}$  and in case of failure it will provide evidence that there are other mechanism determining the in-medium meson production. Indeed, we already know that there are at least other three effects competing with the mean field effect on the  $n/p$  emission. These are the so-called ’’threshold effect’’ emphasized by the calculation of Ref.s [15, 16, 109], the momentum dependence of the isospin-dependent cross sections, and the the isospin mass shift of pions due to the coupling to  $\Delta$ -hole excitation[145]. These will be discussed in the next subsection..

We finally note that a decreasing symmetry term at high density, becoming even negative above  $\simeq 3\rho_0$ , implies more fundamental problems for the stability of a dense isospin asymmetric matter. We can have a collapse as well as  $n/p$  separation instabilities, since the isovector Landau parameter can reach large negative values [1]. No evidence of such effects is present in compact stars as well as in heavy ion collisions.

There are circumstantial reasons to be careful. Indeed, the physics involved in the in-medium particle production has many aspects and a comprehensive and self-consistent approach is necessary before extracting the isospin dependence of the

interaction.

### 7.1. Isospin dependence of thresholds and spectral functions

The "threshold effect" is due to the fact that the masses of nucleons and Delta's are modified in the medium. The unknown self-energies of the delta's are usually specified in terms of the neutron and proton ones by the use of Clebsch-Gordon coefficients for the isospin coupling of the  $\Delta$ 's to nucleons [15, 135]. These medium modifications are isospin dependent, Eq.(13). This influences the phase-space available for meson production in a nucleon-nucleon (NN) collision because it modifies the difference between the invariant energy in the entrance channel  $s_{in}$  with respect to the production threshold  $s_{th}$ . This effect is, of course, present in general for all meson productions, but for brevity we concentrate here on one inelastic channel:  $nm \rightarrow p\Delta^-$ , mainly responsible for  $\pi^-$  production. From Eq.(12) the invariant energy in the entrance channel and the threshold energy are given, respectively, by

$$\begin{aligned} \sqrt{s_{in}}/2 &= [E_n^* + \Sigma_n^0] \xrightarrow{p=0} [m_N^* + \Sigma_\omega^0 + \Sigma_\rho^0 + \Sigma_\delta] > m_N^* + \Sigma_\omega^0 \\ \sqrt{s_{th}} &= [m_p^* + m_{\Delta^-}^* + \Sigma_0(p) + \Sigma_0(\Delta^-)] = [m_N^* + m_\Delta^* + 2\Sigma_\omega] \end{aligned} \quad (16)$$

where  $m_N^*, m_\Delta^*$  are the isospin averaged values. The last equality for the threshold energy is valid due to the prescription for the Delta self-energies, which leads to an exact compensation of the isospin-dependent parts, hence the threshold  $s_{th}$  is not modified by isospin dependent self-energies. In general in a self-consistent many-body calculation higher order effects can destroy this exact balance. But this is not so important for our qualitative discussion, since there will always be a compensating effect in  $s_{th}$ . On the other hand, the energy available in the entrance channel,  $s_{in}$ , is shifted in an explicitly isospin dependent way by the in-medium self-energy  $\Sigma_\rho^0 + \Sigma_\delta > 0$ . Especially, the vector self-energy gives a positive contribution to neutrons that increases the difference  $s_{in} - s_{th}$  and hence increases the cross section of the inelastic process due to the opening up of the phase-space, especially close to threshold, since the intermediate  $\Delta$  resonance will be better probed.

A similar modification but opposite in sign is present in  $s_{in} - s_{th}$  for the  $pp \rightarrow n\Delta^{++}$  channel that therefore is suppressed by the isospin effect on the self-energies. Hence, due to the described threshold effect the ratio  $\pi^-/\pi^+$  increases with the stiffness of  $E_{sym}$  which is associated with a large  $\Sigma_\rho^0 + \Sigma_\delta$ . This is at the origin of the result in Fig.24(left). Of course, the RBUU calculation contains also isospin contributions in the mean field but the final result appears to be dominated by the threshold effect, in particular at lower energies.

However there are at least two other physical aspects that have to be considered. One is the fact that the self-energies in the implementation of RBUU are not explicitly momentum dependent as in DBHF and as the study of the optical potential shows. Thus we return to the importance of the isospin momentum dependence discussed in Sect.5.

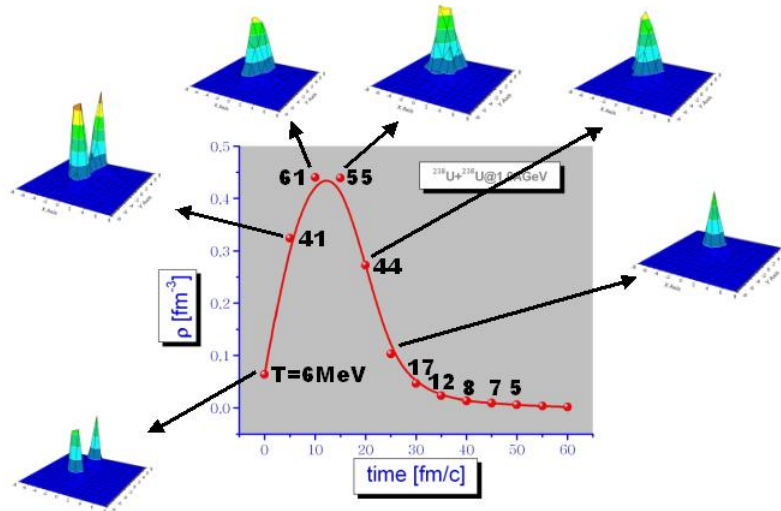


**Figure 25.** (color online)  $^{238}\text{U} + ^{238}\text{U}$ , 1 AGeV, semicentral. Correlation between density, temperature (black values), momentum thermalization (3-D plots), inside a cubic cell, 2.5 fm wide, in the center of mass of the system.

Because we neglect the dependence of the self-energies on momentum, the difference  $s_{in} - s_{th}$  in Eq.(16) increases strongly with the momentum  $p$ . The problem is directly related to the strong energy dependence of the optical potential in RMFT. Therefore it is likely that a more realistic calculation which includes a  $\Sigma_{\rho,\delta}(\rho, p)$  will reduce the effect seen in Fig.24. In addition a fully consistent treatment should include an optical potential also for the pions. It can be envisaged that a stronger sensitivity to  $\Sigma(\rho, p)$  can be seen looking at  $\pi^-/\pi^+$  as a function of the pion transverse energy. Furthermore in a fully self consistent many-body calculation the  $\Sigma$ 's will affect also the isospin dependence of the cross sections for inelastic processes.

Another effect that is certainly present is the modification of the pion spectral function which in an asymmetric medium becomes isospin dependent. This has been recently pointed out in Ref.[145] using a pion interaction in the nuclear medium given by chiral perturbation theory. The effect seems to go in the direction of smaller  $\pi^-/\pi^+$  ratios. Therefore it would be important to include such pion in medium interaction in the transport models, even if it means to go beyond the simple quasi-particle approximation [146].

## 8. Hadron-Quark Transition at High Baryon and Isospin Density

In order to check which kind of matter we are probing in the AGeV beam energy range, also having in mind the possibility of observing some precursor signals of a new physics even in collisions of stable nuclei at intermediate energies, we have performed some event

simulations for the collision of very heavy, neutron-rich, elements. We have chosen the reaction  $^{238}\text{U} + ^{238}\text{U}$  (average proton fraction  $Z/A = 0.39$ ) at  $1\text{ AGeV}$  and semicentral impact parameter  $b = 7\text{ fm}$  just to increase the neutron excess in the interacting region. In Fig.25 we report the evolution of momentum distribution and baryon density in a space cell located in the c.m. of the system, see [22]. We see that after about  $10\text{ fm}/c$  a local equilibration is achieved. We have a unique Fermi distribution and from a simple fit we can evaluate the local temperature (black numbers in MeV). We note that a rather exotic nuclear matter is formed in a transient time of the order of  $10\text{ fm}/c$ , with baryon density around  $3 - 4\rho_0$ , temperature  $50 - 60\text{ MeV}$ , energy density  $500\text{ MeV fm}^{-3}$  and proton fraction between 0.35 and 0.40, see [22]. We can expect some chance of observing signatures of a transition from hadron to quark matter at high baryon and isospin density and relatively low temperature, as discussed in detail in this final Section.

### 8.1. Isospin Effects on the Hadron-Quark Transition at High Density

Several suggestions are already present about the possibility of interesting isospin effects on the transition to a mixed hadron-quark phase at high baryon density [21, 22, 109]. This seems to be a very appealing physics program for the new facilities, FAIR at GSI-Darmstadt [147] and NICA at JINR-Dubna [148], where heavy ion beams (even unstable, with large isospin asymmetry) will be available with good intensities in the 1-30 AGeV energy region.

The weak point of those predictions is the lack of a reliable equation of state that can describe with the same confidence the two phases, hadronic and deconfined. On the other hand this also represents a strong theory motivation to work on more refined effective theories for a strong interacting matter.

A nice qualitative argument in favor of noticeable isospin effects on the hadron-quark transition at high density can be derived from the Fig.26, where we compare typical Equations of State (EoS) for Hadron (Nucleon) and Quark Matter, at zero temperature, for symmetric ( $\alpha \equiv (\rho_n - \rho_p)/\rho_B \equiv -\rho_3/\rho_B = 0.0$ ) and neutron matter ( $\alpha = 1.0$ ), where  $\rho_{n,p}$  are the neutron/proton densities and  $\rho_B = \rho_n + \rho_p$  the total baryon density. For the Hadron part we adopt a Relativistic Mean Field EoS (Sects.6-7) with non-linear terms and an effective  $\rho$ -meson coupling for the isovector part, largely used to study isospin effects in relativistic *HIC* (Sect.7) [149].

The energy density and the pressure for the quark phase are given by the MIT Bag model [152] (two-flavor case), with the bag constant taken as a rather standard value from the hadron spectra ( $B = 85.7\text{ MeV fm}^{-3}$ , no density dependence) [153].

The transition to the more repulsive quark matter will appear around the crossing points of the two EoS. We see that such crossing for symmetric matter ( $\alpha_H = \alpha_Q = 0.0$ ) is located at rather high density,  $\rho_B \simeq 7\rho_0$ , while for pure neutron matter ( $\alpha_H = \alpha_Q = 1.0$ ) it is moving down to  $\rho_B \simeq 3\rho_0$ . Of course Fig.26 represents just a simple energetic argument to support the hadron-quark transition to occur at lower baryon densities for more isospin asymmetric matter. In the following we will rigourously consider the case

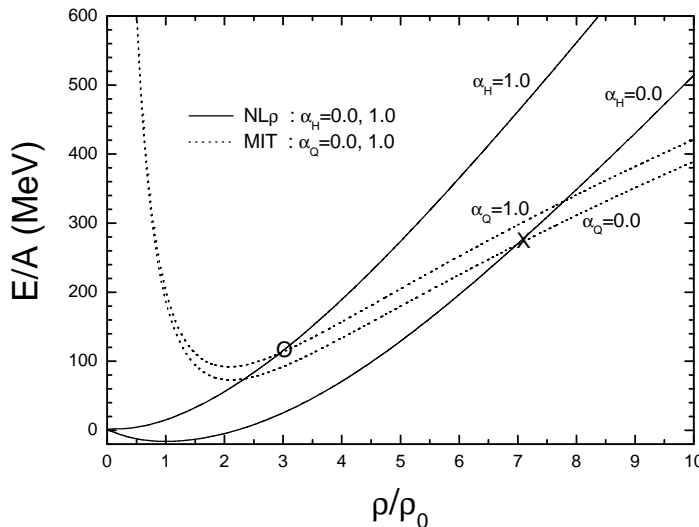


**Figure 26.** Zero temperature  $EoS$  of Symmetric/Neutron Matter: Hadron ( $NL\rho$ ), solid lines, vs. Quark (MIT-Bag), dashed lines.  $\alpha_{H,Q}$  represent the isospin asymmetry parameters respectively of the hadron, quark matter:  $\alpha_{H,Q} = 0$ , Symmetric Matter;  $\alpha_{H,Q} = 1$ , Neutron Matter.

of a first order phase transition in the Gibbs frame for a system with two conserved charges (baryon and isospin), in order to derive more detailed results. Since the first order phase transition presents a jump in the energy, we can expect the mixed phase to start at densities even before the crossing points of the Fig.1. The lower boundary then can be predicted at relatively low baryon densities for asymmetric matter, likely reached in relativistic heavy ion collisions and in compact stars. In fact this point is certainly of interest for the structure of the crust and the inner core of Neutron Stars (NS), e.g. see refs. [154, 155] and the review [17]. We like to mention a very recent estimation of the NS Mass-Radius correlation ( $1.6M_{sun} - 10Km$ ) with high confidence level, that could indicate a transition to quark matter in the inner core [156].

We finally note that the above conclusions are rather independent on the isoscalar part of the used Hadron EoS at high density, that is chosen to be rather soft in agreement with collective flow and kaon production data [23, 137].

In the used Bag Model no gluon interactions, the  $\alpha_s$ -strong coupling parameter, are included. We remark that this in fact would enhance the above effect, since it represents an attractive correction for a fixed B-constant, see [157]. A reduction of the Bag-constant with increasing baryon density, as suggested by various models, see ref.[154], will also go in the direction of an “earlier” (lower density) transition, as already seen in ref.[22]. At variance, the presence of explicit isovector interactions in the quark phase could play an important role, as shown in the following also for other isospin properties inside the mixed phase.

### 8.2. Isospin effects on the Mixed Phase

We can study in detail the isospin dependence of the transition densities [21, 22, 109].

The structure of the mixed phase is obtained by imposing the Gibbs conditions [158] for chemical potentials and pressure and by requiring the conservation of the total baryon and isospin densities:

$$\begin{aligned}
 \mu_B^H(\rho_B^H, \rho_3^H, T) &= \mu_B^Q(\rho_B^Q, \rho_3^Q, T) , \\
 \mu_3^H(\rho_B^H, \rho_3^H, T) &= \mu_3^Q(\rho_B^Q, \rho_3^Q, T) , \\
 P^H(T)(\rho_B^H, \rho_3^H, T) &= P^Q(T)(\rho_B^Q, \rho_3^Q, T) , \\
 \rho_B &= (1 - \chi)\rho_B^H + \chi\rho_B^Q , \\
 \rho_3 &= (1 - \chi)\rho_3^H + \chi\rho_3^Q ,
 \end{aligned} \tag{17}$$

where  $\chi$  is the fraction of quark matter in the mixed phase and  $T$  is the temperature.

The consistent definitions for the densities and chemical potentials in the two phases are given by :

$$\begin{aligned}
 \rho_B^H &= \rho_p + \rho_n, & \rho_3^H &= \rho_p - \rho_n , \\
 \mu_B^H &= \frac{\mu_p + \mu_n}{2}, & \mu_3^H &= \frac{\mu_p - \mu_n}{2} ,
 \end{aligned} \tag{18}$$

for the Hadron Phase and

$$\begin{aligned}
 \rho_B^Q &= \frac{1}{3}(\rho_u + \rho_d) , & \rho_3^Q &= \rho_u - \rho_d , \\
 \mu_B^Q &= \frac{3}{2}(\mu_u + \mu_d), & \mu_3^Q &= \frac{\mu_u - \mu_d}{2} ,
 \end{aligned} \tag{19}$$

for the Quark Phase.

The related asymmetry parameters are:

$$\alpha^H \equiv -\frac{\rho_3^H}{\rho_B^H} = \frac{\rho_n - \rho_p}{\rho_n + \rho_p} , \quad \alpha^Q \equiv -\frac{\rho_3^Q}{\rho_B^Q} = 3\frac{\rho_d - \rho_u}{\rho_d + \rho_u} . \tag{20}$$

Nucleon and quark chemical potentials, as well as the pressures in the two phases, are directly derived from the respective EoS.

In this way we get the *binodal* surface which gives the phase coexistence region in the  $(T, \rho_B, \rho_3)$  space. For a fixed value of the total asymmetry  $\alpha_T = -\rho_3/\rho_B$  we will study the boundaries of the mixed phase region in the  $(T, \rho_B)$  plane. Since in general the charge chemical potential is related to the symmetry term of the EoS, [1],  $\mu_3 = 2E_{sym}(\rho_B)\frac{\rho_3}{\rho_B}$ , we expect critical and transition densities rather sensitive to the isovector channel in the two phases.

In the hadron sector we use the NL-RMF models, Sects.6-7, with different structure of the isovector part: i) *NL*, where no isovector meson is included and the symmetry term is only given by the kinetic Fermi contribution, ii) *NLρ* when the interaction contribution of an isovector-vector meson is considered and finally iii) *NLρδ* where also

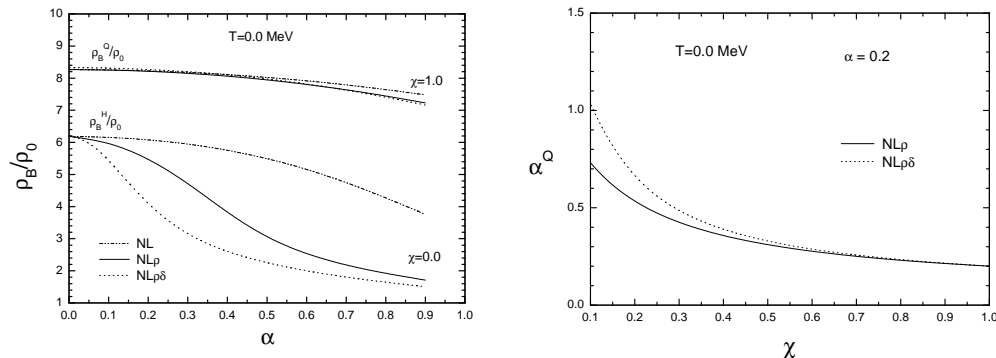


**Figure 27.** Left Panel. Dependence on the Hadron Symmetry Energy of the Lower ( $\chi = 0.0$ ) and Upper ( $\chi = 1.0$ ) Boundaries of the Mixed Phase, at zero temperature, vs. the asymmetry parameter.

Right Panel. Quark asymmetry in the mixed phase vs. the quark concentration for asymmetric matter with  $T = 0$  and  $\alpha = 0.2$ .  $NL\rho$  and  $NL\rho\delta$  Effective Hadron Interactions are considered.

Quark *EoS*: MIT bag model with  $B^{1/4} = 160 \text{ MeV}$ .

the contribution of an isovector-scalar meson is accounted for. At high baryon densities the symmetry energy is increasing in a different way with the various choices, see Sect.6, and we will look at the effect on the phase transition.

As already mentioned, in the quark phase we use the MIT-Bag Model, where the symmetry term is only given by the Fermi contribution. The Bag parameter  $B$  is fixed for each baryon density to a constant, rather standard, value  $B^{1/4} = 160 \text{ MeV}$ , corresponding to a Bag Pressure of  $85.7 \text{ MeV fm}^{-3}$ .

In general for each effective interactive Lagrangian we can simulate the solution of the highly non-linear system of Eqs.(17), via an iterative minimization procedure, in order to determine the binodal boundaries and eventually the Critical End Point (CEP) ( $T_c, \rho_c^B$ ) of the mixed phase.

A relatively simple calculation can be performed at zero temperature. The isospin effect (asymmetry dependence) on the Lower ( $\chi = 0.0$ ) and Upper ( $\chi = 1.0$ ) transition densities of the Mixed Phase are shown in Fig.27(Left Panel) for various choices of the Hadron EoS. The effect of a larger repulsion of the symmetry energy in the hadron sector, from  $NL$  to  $NL\rho$  and to  $NL\rho\delta$ , is clearly evident on the lower boundary with a sharp decrease of the transition density even at relatively low asymmetries.

Typical results for isospin effects on the whole binodal “surface” are presented in Fig.28 for  $\alpha = 0.2$  asymmetric matter. As expected, the lower boundary of the mixed phase is mostly affected by isospin effects. In spite of the relatively small total asymmetry, we clearly see a shift to the left of the first transition boundary, in particular at low temperature, and a relatively “early” Critical End Point. In fact from the present results we cannot exclude a *CEP* at higher temperature and smaller baryon density, as suggested by other similar calculations [21]. However we have also to mention some

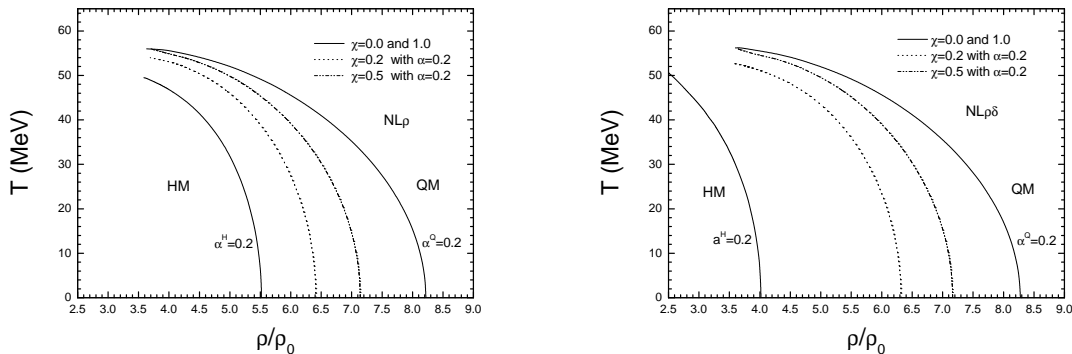


**Figure 28.** Asymmetric  $\alpha = 0.2$  matter. Binodal surface and  $(T, \rho_B)$  curves for various quark concentrations ( $\chi = 0.2, 0.5$ ) in the mixed phase. Hadron *EoS*:  $NL\rho$  Effective Interaction (Left Panel);  $NL\rho\delta$  Effective Interaction (Right Panel). Quark *EoS*: MIT Bag model with  $B^{1/4} = 160$  MeV.

numerical problems. The solution of the Gibbs conditions, the highly non-linear system of Eqs.(17), is found through an iterative multi-parameter minimization procedure (the Newton-Raphson method). When we are close to the Critical End Point, for each  $\chi$ -concentration the baryon and isospin densities of the hadron and quark phases become very similar and we start to have problems in finding a definite minimum.

In the following we will concentrate on properties of the mixed phase mostly located at high density and relatively low temperature, well described in the calculation and within the reach of heavy ion collisions in the few AGeV range, see the discussion around Fig.25. We note that high intensity  $^{238}\text{U}$  beams in this energy range will be available in the first stage of the FAIR facility [147, 159] and also at JINR-Dubna in the Nuclotron first step of the NICA project [162].

### 8.3. Inside the Mixed Phase of Asymmetric Matter

For  $\alpha = 0.2$  asymmetric matter, in the Fig.28 we show also the  $(T, \rho_B)$  curves inside the Mixed Phase corresponding to a 20% and 50% presence of the quark component ( $\chi = 0.2, 0.5$ ), evaluated respectively with the two choices,  $NL\rho$  (Left Panel) and  $NL\rho\delta$  (Right Panel), of the symmetry interaction in the hadron sector. We note, as also expected from Fig.27, that in the more repulsive  $NL\rho\delta$  case the lower boundary is much shifted to the left. However this effect is not so evident for the curve corresponding to a 20% quark concentration, and almost absent for the 50% case. The conclusion seems to be that for a stiffer symmetry term in a heavy-ion collision at intermediate energies during the compression stage we can have more chance to probe the mixed phase, although in a region with small weight of the quark component.

Can we expect some signatures related to the subsequent hadronization in the following expansion?

An interesting possibility is coming from the study of the asymmetry  $\alpha^Q$  in the

quark phase. In fact since the symmetry energy is rather different in the two phases we can expect an Isospin Distillation (or Fractionation), very similar to the one observed in the Liquid-Gas transition in dilute nuclear matter [9, 1, 33], this time with the larger isospin content in the higher density quark phase.

In Fig.27 (Right Panel) we show the asymmetry  $\alpha^Q$  in the quark phase as a function of the quark concentration  $\chi$  for the case with global asymmetry  $\alpha = 0.2$  (zero temperature). The calculation is performed with the two choices of the symmetry term in the hadron sector. We see an impressive increase of the quark asymmetry when we approach the lower boundary of the mixed phase. Of course the quark asymmetry recovers the global value 0.2 at the upper boundary  $\chi = 1$ . A simple algebraic calculation allows to evaluate the corresponding asymmetries of the hadron phase. In fact from the charge conservation we have that for any  $\chi$ -mixture the global asymmetry  $\alpha$  is given by:

$$\alpha \equiv -\frac{\rho_3}{\rho_B} = \frac{(1-\chi)\alpha^H}{(1-\chi) + \chi\frac{\rho_B^Q}{\rho_B^H}} + \frac{\chi\alpha^Q}{(1-\chi)\frac{\rho_B^H}{\rho_B^Q} + \chi} \quad (21)$$

For any  $\chi$ , from the calculated  $\alpha^Q$  of Fig.27 (Right) and the  $\rho_B^H, \rho_B^Q$  obtained from the Gibbs Eqs.(17), we can get the correspondent asymmetry of the hadron phase  $\alpha^H$ . For a 20% quark concentration we have an  $\alpha^Q/\alpha^H$  ratio around 5 for  $NL\rho$  and around 20 for  $NL\rho\delta$ , more repulsive in the isovector channel [153]. It is also interesting to compare the isospin content  $N/Z$  of the high density region expected from transport simulations without the Hadron-Quark transition and the effective  $N/Z$  of the quark phase in a 20% concentration. In the case of  $Au + Au$  (initial  $N/Z = 1.5$ ) central collisions at  $1AGeV$  in pure hadronic simulations we get in the high density phase a reduced  $N/Z \sim 1.2 - 1.25$  (respectively with  $NL\rho\delta - NL\rho$  interactions) due to the fast neutron emission [16, 35]. In presence of the transition, the corresponding isospin content of the quark phases is much larger,  $N/Z = 3$  for  $NL\rho$  and  $N/Z = 5.7$  for  $NL\rho\delta$ . This is the *neutron trapping* effect. We expect a signal of such large asymmetries, coupled to a larger baryon density in the quark phase, in the subsequent hadronization. We could predict an enhancement of the production of isospin-rich nucleon resonances and subsequent decays, i.e. an increase of  $\pi^-/\pi^+$ ,  $K^0/K^+$  yield ratios for reaction products coming from high density regions, that could be selected looking at large transverse momenta, corresponding to a large radial flow.

If such kinetic selection of particles from the mixed phase can really be successful also other mixed phase signatures would become available. One is related to the general softening of the matter, due to the contribution of more degrees of freedom, that should show up in the damping of collective flows [160].

The azimuthal distributions (elliptic flows) will be particularly affected since particles mostly retain their high transverse momenta escaping along directions orthogonal to the reaction plane without suffering much rescattering processes. A further signature could be the observation, for the selected particles, of the onset of a quark-number scaling of the elliptic flow: a property of hadronization by quark coalescence

that has been predicted and observed at RHIC energies, i.e. for the transition at  $\mu_B = 0$  [161].

We finally remark that at higher temperature and smaller baryon chemical potential (ultrarelativistic collisions) the isospin effects discussed here are expected to vanish [162], even if other physics can enter the game and charge asymmetry effects are predicted also at  $\mu_B = 0$  and  $T \simeq 170 \text{ MeV}$  [163, 164].

#### 8.4. Isospin in Effective Quark Models

From the above discussion it clearly appears that the lack of explicit isovector interactions in the quark sector could strongly affect the location of the phase transition in asymmetric matter and the related expected observables. So it seems extremely important to include the Isospin degree of freedom in any effective QCD dynamics. A first approach can be supplied by a two-flavor Nambu-Jona Lasinio (*NJL*) model [165] where the isospin asymmetry can be included in a flavor-mixing picture [166, 167]. These isospin effects are induced by a determinant interaction related to the breaking of the axial symmetry. The new Gap Equations are like  $M_i = m_i - 4G_1\Phi_i - 4G_2\Phi_j$ ,  $i \neq j$ , ( $u, d$ ), where the  $\Phi_{u,d} = \langle \bar{u}u \rangle$ ,  $\langle \bar{d}d \rangle$  are the two (negative) condensates and  $m_{u,d} = m$  the (equal) current masses. Introducing explicitly a flavor mixing, i.e. the dependence of the constituent mass of a given flavor to both condensate, via  $G_1 = (1 - \eta)G_0$ ,  $G_2 = \eta G_0$  we have the coupled equations

$$\begin{aligned} M_u &= m - 4G_0\Phi_u + 4\eta G_0(\Phi_u - \Phi_d), \\ M_d &= m - 4G_0\Phi_u + 4(1 - \eta)G_0(\Phi_u - \Phi_d). \end{aligned} \quad (22)$$

For  $\eta = 1/2$  we have back the usual NJL ( $M_u = M_d$ ), while small/large mixing is for  $\eta \Rightarrow 0/\eta \Rightarrow 1$  respectively.

In neutron rich matter  $|\Phi_d|$  decreases more rapidly due to the larger  $\rho_d$  and so  $(\Phi_u - \Phi_d) < 0$ . In the “realistic” small mixing case, see also [166, 168], we will get a definite  $M_u > M_d$  splitting at high baryon density (before the chiral restoration). This expectation is nicely confirmed by a full calculation [169] of the coupled gap equations with standard parameters (same as in ref.[166]).

All that can indicate a more fundamental confirmation of the  $m_p^* > m_n^*$  splitting in the hadron phase, as suggested by the effective *QHD* model with the isovector scalar  $\delta$  coupling, see [1, 34] and Sects.5, 6.

However such isospin mixing effect results in a very small variation of the symmetry energy in the quark phase, still related only to the Fermi kinetic contribution. In fact this represents just a very first step towards a more complete treatment of isovector interactions in effective quark models, of large interest for the discussion of the phase transition at high densities. We remind that confinement is still missing in these mean field approaches.

More generally starting from the QCD Lagrangian one can arrive to an effective color current-current interaction where an expansion in various components can provide

isovector contributions [170]. We also notice the evidence that chiral symmetry restoration is favored in systems with large neutron excess [171].

A very interesting point has been recently suggested about the possibility of a quark matter formed in a color superconducting state [172]. A strong symmetry repulsion comes from the fact that equal densities of up and down quarks are energetic favored to allow the formation of a diquark condensate. This will be in competition with a decreasing of the diquark pairing at large isospin asymmetries. Exciting new perspectives are opening up.

In conclusion the aim of this project is twofold:

- To stimulate new experiments on isospin effects in heavy ion collisions at intermediate energies (in a few  $AGeV$  range) with attention to the isospin content of produced particles and to elliptic flow properties, in particular for high- $p_t$  selections.
- To stimulate more refined models of effective Lagrangians for non-perturbative QCD, where isovector channels are consistently accounted for.

## 9. Perspectives and Suggested Observables

We have shown how dissipative Heavy Ion Collisions with charge asymmetric isotopes provide a valuable, in fact unique, tool to extend our knowledge of the Nuclear Matter Phase Diagram along the "third" isovector component,  $\rho_3 = \rho_n - \rho_p$ . Due to the low asymmetries reached in terrestrial laboratories, even with unstable beams, it is difficult to disentangle density and momentum dependence of the in-medium symmetry potentials from the corresponding properties of the isoscalar interactions. Therefore our discussion has been mainly focused on exclusive experiments, where suitable correlations can better isolate isovector effects.

The fundamental microscopic tool to relate isospin properties of the reaction products to the underlying interaction is the transport theory to describe the evolution of the reaction dynamics. We must remark that isoscalar global properties of the collision dynamics (like stopping power and density variations, pre-equilibrium emissions and main reaction mechanisms) should be correctly reproduced otherwise also the isovector predictions will be not fully reliable. We remind that one of the most important information is about the density dependence of the symmetry energy away from saturation. This is in fact a basic requirement for a comparison of different transport models.

We have used a non-relativistic and relativistic Stochastic Mean Field approach. In this way we can account for the very important Mean Field Dynamics coupled to Fluctuation Terms that can lead to fragment formation in mechanical/chemical unstable regions, and in general to the onset of various other instabilities, as well as to the widths in the distributions of the measured quantities.

We have selected some relevant features of the Isospin Dynamics:

- a) Collective Isospin Equilibration (Sect.3)

- b) Isospin Diffusion due to asymmetry gradients (Sect.4.1)
- c) Isospin Distillation in multifragmentation (Sect.4.2)
- d) Isospin Migration due to density gradients (Sect.4.3)
- e) Isospin flows and isospin effects on nucleon, cluster and meson production at high energies (Sects. 5 and 7)
- f) Isospin effects on the Mixed Phase in the hadron-quark transition at high baryon density (Sect.8)

In correspondence we have suggested the more promising exclusive measurements:

1. Angular distribution of the prompt dipole radiation, measured with high-intensity n-rich ions, like  $^{132}\text{Sn}$ .
2. Correlation between isospin diffusion and total energy loss, which gives a direct measure of the interacting time.
3. Correlation between fragment isospin content and radial velocity, possibly with a reconstruction of the primary fragments (in particular the neutron emission).
4. Angular, mass and velocity correlations of the isospin properties of the neck fragments.
5. Transverse momentum analysis of the isospin content of nucleon, clusters and mesons emitted at mid rapidity in intermediate energy collisions, and of the corresponding collective flows.
6. High  $p_t$  study of the quenching of hadron elliptic flows joined to some evidence of the "neutron trapping" effect (enhancement of production of isospin-rich nucleon resonances and subsequent decays) as indicator of the formation of a mixed hadron-quark phase.

From the present available data at the Fermi energies we can deduce a rather stiff (close to a linear behavior) symmetry energy below/around the saturation density, from points b), c), d). Similar indications are appearing from point e) concerning the higher density regions. Here the isospin effects on the momentum dependence (splitting of the nucleon effective masses) seem to be also relevant. Very nice perspectives are opening up with the new facilities, even for unstable beams, soon operating at higher energies.

### *Acknowledgments*

On some of the topics presented here we warmly thank the fruitful and pleasant collaboration of very nice people: G.Ferini, Th.Gaitanos, V.Giordano, B.Liu, F.Matera, S.Plumari, V.Prassa, C.Rizzo, J.Rizzo, M.Zielinska-Pfabe and H.H.Wolter. We acknowledge several inspiring discussions with theory and experiment colleagues: D.Blaschke, B.Borderie, Ph.Chomaz, P.Danielewicz, E.De Filippo, E.Galichet, C.M.Ko, B.A.Li, Qinfeng Li, W.G.Lynch, A.Pagano, J.Randrup, W.Reisdorf, M.F.Rivet, P.Russotto, D.V.Shetty, C.Simenel, H.Stoecker, W.Trautmann, M.B.Tsang, S.Typel, J.Wilczynski and S.J.Yennello.

One of the authors, V. B. thanks for warm hospitality at Laboratori Nazionali del Sud, INFN. This work was supported in part by the Romanian Ministry for Education

and Research under the CNCSIS contract PN II ID-946/2007 and CNMP grant PNII-Partnerships No. 71-073/2007-PROPETHAD.

## References

- [1] Baran V, Colonna M, Greco V and Di Toro M 2005 *Phys. Rep.* **410** 335-466.
- [2] Fuchs C, Wolter HH, *Eur. Phys. Jour.* 2006 **A30** 5.
- [3] Fantoni S et al., 2008 AIP Conf.Proc. **1056** 233-240 and arXiv:0807.543[nucl-th]  
Gandolfi S et al., 2009 *Phys. Rev.* **C79** 054006.
- [4] van Dalen E, Muether H, 2010 *Relativistic Effects in Nuclear Matter and Nuclei*, arXiv:1004.0144[nucl-th].
- [5] Klimkiewicz A et al., 2007 *Phys. Rev.* **C76** 051603(R).
- [6] Piekarewicz J, 2006 *Phys. Rev.* **C73** 044325.
- [7] Trippa L, Colo' G, Vigezzi E, 2008 *Phys. Rev.* **C77** 061304.
- [8] Carbone A, Colo' G, Bracco A, Bortignon PF, Camera F, Wieland O, 2010 *Constraints on the symmetry energy and on neutron skins from the pigmy resonances in  $^{68}\text{Ni}$  and  $^{132}\text{Sn}$* , *Phys. Rev. C* in press.
- [9] Baran V, Colonna M, Di Toro M and Larionov A 1998 *Nucl. Phys. A* **632** 287-303.
- [10] Tsang MB et al., 2004 *Phys. Rev. Lett.* **92** 062701
- [11] Horowitz CJ, Piekarewicz J, 2002 *Phys. Rev.* **C66** 055803
- [12] Steiner A, Prakash M, Lattimer JM, Ellis PJ, 2005 *Phys. Rep.* **441** 325
- [13] Greco V et al. 2003 *Phys. Lett.B* **562** 215.
- [14] Li BA, Chen LW, Ko CM, 2008 *Phys. Rep.* **465** 113.
- [15] Ferini G, Colonna M, Gaitanos T, Di Toro M, 2005 *Nucl. Phys.* **A762** 147
- [16] Ferini G, Gaitanos T, Colonna M, Di Toro M and Wolter H H 2006 *Phys. Rev. Lett.* **97** 202301.
- [17] Page D and Reddy S 2006 *Ann. Rev. Nucl. Part. Sci.* **56** 327.
- [18] Lattimer JM, Prakash M, 2007 *Phys. Rep.* **442** 109
- [19] Prakash M, 2007 *J. Phys. G* **34** 253,  
2008 arXiv:0812.2002, *Int. Conf. Nuclei in the Cosmos*
- [20] Baldo M, Burgio GF, Castorina P, Plumari S, Zappala' D, 2007 *Phys. Rev.* **C75** 035804
- [21] Müller H 1997 *Nucl. Phys. A* **618** 349.
- [22] Di Toro M, Drago A, Gaitanos T, Greco V and Lavagno A 2006 *Nucl. Phys. A* **775** 102.
- [23] Danielewicz P, Lacey R and Lynch W G 2002 *Science* **298** 1592.
- [24] Colonna M, Di Toro M, Fabbri G, Maccarone S, 1998 *Phys. Rev.* **C57** 1410
- [25] Li BA, Ko CM, Bauer W, 1998 *Int. J. Mod. Phys.* **E7** 147
- [26] *Isospin Physics in Heavy-ion Collisions at Intermediate Energies*, Eds. Li BA and Schröder WU, Nova Science Publishers (2001, New York)
- [27] Baran V, Colonna M, Di Toro M, 2004 *Nucl. Phys.* **A730** 329.
- [28] Di Toro M, Olmi A, Roy R, 2006 *Eur. Phys. Jour.* **A30** 65
- [29] Colonna M and Tsang MB, 2006 *Eur. Phys. J.* **A30** 165, and refs. therein.
- [30] Shetty DV, Yennello SJ, 2010 *Nuclear Symmetry Energy: an experimental overview*, arXiv:1002.0313[nucl-ex]
- [31] Guarnera A, Colonna M, Chomaz P, 1996 *Phys. Lett.* **B373** 267.
- [32] Colonna M et al., 1998 *Nucl. Phys.* **A642** 449.
- [33] Chomaz P, Colonna M and Randrup J 2004 *Phys. Rep.* **389** 263-440.
- [34] Liu B, Greco V, Baran V, Colonna M, and Di Toro M 2002 *Phys. Rev.* **C65** 045201.
- [35] Gaitanos T et al. 2004 *Nucl. Phys.A* **732** 24.
- [36] Santini E, Gaitanos T, Colonna M, Di Toro M, 2005 *Nucl. Phys.* **A756** 468.
- [37] Typel S, Roepke G, Klaehn T, Blaschke D, Wolter HH, 2010 *Phys. Rev.* **C81** 015803.

- [38] Natowitz J et al., 2010 *Symmetry Energy of Dilute Warm Nuclear Matter*, arXiv:1001.1102[nucl-th].
- [39] Ayik S, Gregoire C, 1988 *Phys. Lett.* **B212** 269, and refs. therein.
- [40] Randrup J, Remaud B, 1990 *Nucl. Phys.* **A514**, 339
- [41] Baran V et al., 2002 *Nucl. Phys.* **A703** 603
- [42] Rizzo J et al., 2004 *Nucl. Phys.* **A732** 202.
- [43] Di Toro M, Colonna M, Rizzo M, 2005 *AIP Conf. Proc.* **791** 70-83.
- [44] Rizzo J, 2006 *Collective and Stochastic Observables in HIC at Intermediate Energies* Ph.D. Thesis, Univ. Catania
- [45] Rizzo J, Colonna M, Di Toro M, 2005 *Phys. Rev.* **C72** 064609.
- [46] Rizzo J et al., 2008 *Nucl. Phys.* **A806** 79-104.
- [47] Gale C, Bertsch GF, Das Gupta S, 1987 *Phys. Rev.* **C35** 1666
- [48] Gale C, Welke GM, Prakash M, Lee SJ, Das Gupta S, 1990 *Phys. Rev.* **C41** 1545.
- [49] Bombaci I et al., 1995 *Nucl. Phys.* **A583** 623.
- [50] Greco V, 1997 Master Thesis, Catania Univ.;
- Greco V, Guarnera A, Colonna M, Di Toro M, 1999 *Phys. Rev.* **C59** 810;  
1998 *Nuovo Cimento* **A111** 865.
- [51] Li BA, Das CB, Das Gupta S, Gale C, 2004 *Nucl. Phys.* **A735** 563
- [52] Giordano V, Colonna M, Di Toro M, Greco V, Rizzo J, 2010 *Isospin emission and flow at high baryon density: a test of the symmetry potential* arXiv:1001.4961 [nucl-th]
- [53] Berlinger M et al., 1979 *Z. Phys.* **A291** 133
- [54] Hernandez ES et al., 1981 *Nucl. Phys.* **A361** 483
- [55] Bonche P, Ngo N, 1981 *Phys. Lett.* **B105** 17
- [56] Di Toro M, Gregoire C, 1985 *Z. Phys.* **A320** 321
- [57] Suraud E, Pi M, Schuck P, 1989 *Nucl. Phys.* **A492** 294
- [58] Brink DM, 1990 *Nucl. Phys.* **A519** 3
- [59] Chomaz P, Di Toro M, Smerzi A, 1993 *Nucl. Phys.* **A563** 509
- [60] Bortignon PF et al., 1995 *Nucl. Phys.* **A583** 101c.
- [61] Pierroutsakou D et al., 2005 *Phys. Rev.* **C71** 054605
- [62] Martin B, Pierroutsakou D et al. (Medea Collab.), 2008 *Phys. Lett.* **664** 47
- [63] Brink DM, Di Toro M, 1981 *Nucl. Phys.* **A372** 151
- [64] V. Baran et al., *Nucl. Phys.* **A600** (1996) 111.
- [65] C. Simenel et al., *Phys. Rev. Lett.* **86** (2000) 2971.
- [66] Baran V, Brink DM, Colonna M, Di Toro M, 2001 *Phys. Rev. Lett.* **87** 182501
- [67] Simenel C, Chomaz P, de France G, 2001 *Phys. Rev. Lett.* **86** 2971  
and 2007 *Phys. Rev.* **C76** 024609
- [68] Di Toro M et al., 2008 *Int.Jou.Mod.Phys.* **E17** 110
- [69] Lewitowicz M, 2008 *Nucl.Phys.* **A805** 519c
- [70] Letter of Intent for the new SPIRAL2 Facility at GANIL.
- [71] Baran V, Rizzo C, Colonna M, Di Toro M, Pierroutsakou D, 2009 *Phys. Rev.* **C79** 021603(R)
- [72] Famiano M et al., 2006 *Phys. Rev. Lett.* **97** 052701
- [73] Zielinska-Pfabe M et al, 2008 *Isospin Properties of fast Light Particles*, IWM Int.Workshop, SIF, Conf.Proc.Vol. **95** p. 303-310.
- [74] Mueller H, Serot BD, 1995 *Phys. Rev.* **C52** 2072
- [75] Li BA, Ko CM, 1997 *Nucl.Phys.* **A618** 498
- [76] Baran V, Colonna M, Di Toro M, Greco V, 2001 *Phys. Rev. Lett.* **86** 4492
- [77] Margueron J, Chomaz P, 2003 *Phys. Rev.* **C67** 041602
- [78] Wuenschel S et al., 2009 *Phys. Rev.* **C79** 061602.
- [79] Li BA, Chen LW, 2005 *Phys. Rev.* **C72** 064611;  
Chen LW, Ko CM, Li BA, 2005 *Phys. Rev. Lett* **94** 032701.
- [80] Souliotis GA, Velselsky M, Shetty DV, Yennello SJ, 2004 *Phys. Lett.* **B588** 35

- [81] Galichet E et al., 2009 *Phys. Rev.* **C79** 064615.
- [82] Galichet E et al., 2009 *Phys. Rev.* **C79** 064614.
- [83] Durand D, 1992 *Nucl.Phys.* **A541** 266
- [84] Tsang MB et al., 2009 *Phys. Rev. Lett.* **102** 122701.
- [85] Amorini F. et al., 2009 *Phys. Rev. Lett.* **102** 112701.
- [86] Rami F et al., 2000 *Phys. Rev. Lett.* **84** 1120
- [87] We note that the Imbalance Ratio appears also not dependent on pre-equilibrium emissions as well as on secondary decays [10, 46].
- [88] Colonna M, Baran V, Di Toro M, Wolter HH, 2008 *Phys.Rev.* **C78** 064618
- [89] Li BA, Chen LW, Yon GC, Zuo W, 2006 *Phys. Lett.* **B634** 378
- [90] H.S.Xu et al., 2000 *Phys. Rev. Lett.* **85** 716
- [91] Li BA, Ko CM, Ren Z, 1997 *Phys.Rev.Lett.* **78** 1644
- [92] Liu TX et al., 2004 *Phys. Rev.* **C69** 014603
- [93] Colonna M, Fabbri G, Di Toro M, Matera F, Wolter HH, 2004 *Nucl. Phys.* **A742** 337
- [94] Frankland JD et al., 2001 *Nucl. Phys.* **A689** 940
- [95] Colonna M, Di Toro M, Guarnera A, 1995 *Nucl. Phys.* **A589** 160.
- [96] Baran V, Colonna M, Di Toro M, Zielinska-Pfabe M, Wolter HH, 2005 *Phys. Rev.* **C72** 064620.
- [97] Piantelli P et al., 2006 *Phys. Rev.* **C74** 034609.
- [98] Piantelli P et al., 2007 *Phys. Rev.* **C76** 061601.
- [99] Milazzo P et al., 2005 *Nucl. Phys.* **A756** 39.
- [100] Theriault D et al., 2006 *Phys. Rev.* **C74** 051602.
- [101] Hudan S et al., 2005 *Phys. Rev.* **C71** 054604.
- [102] De Filippo E et al.(Chimera Collab.), 2005 *Phys. Rev.* **C71** 044602  
2005 *Phys. Rev.* **C71** 064604
- [103] Russotto P et al. (Chimera Coll.), 2006 *Int. J. Mod. Phys.* **E15** 410.
- [104] Wilczynski J et al. (Chimera Collab.), 2005 *Int. Jour. Mod. Phys.* **E14** 353.
- [105] Papa M et al., 2007 *Phys. Rev.* **C75** 054616.
- [106] Hudan S, deSouza RT and A. Ono A, 2006 *Phys. Rev.* **C73** 054602.
- [107] Planeta R et al., 2008 *Phys. Rev.* **C77** 014610.
- [108] De Filippo E et al. (Chimera Collab.), 2006, *Time scales and isospin effects on reaction dynamics*, NN06 Conf., Rio de Janeiro,  
2009, *Acta Physica Polonica* **B40** 1199
- [109] Di Toro M et al. 2009 *Progr. Part. Nucl. Phys.* **62** 389-401.
- [110] Li T, Garg U et al., 2007 *Phys. Rev. Lett.* **99** 162503.
- [111] Colin J et al. (INDRA Coll.), 2003 *Phys. Rev.* **C67** 064603.
- [112] Lynch WG et al., 2009 *Prog. Part. Nucl. Phys.* **62** 427
- [113] A.A. Stefanini AA et al., 1995 *Z. Phys.* **A351** 167.
- [114] Wilczynski J et al, (CHIMERA Coll.), 2005 *Int. J. Mod. Phys.* **E14** 353.
- [115] Lioni R, Baran V, Colonna M, Di Toro M, 2005 *Phys. Lett.* **B625** 33.
- [116] De Filippo E et al.(CHIMERA Coll.), 2009, Invited talk at IWM09, Catania, Italy. (to be published).
- [117] Bombaci I, Lombardo U, 1991 *Phys. Rev.* **C44** 1892.
- [118] Reisdorf W and FOPI Collab., 2009 private communication and ECT\*-Trento Workshop *HIC at Low and Intermediate Energies*, May 09, on the Web.
- [119] Danielewicz P, 2000 *Nucl. Phys.* **A673** 375.
- [120] Li Q, Li Z, Soff S, Bleicher M, Stoecker H, 2005 *Phys. Rev.* **C72** 034613;  
Li Q, Li Z, Stoecker H, 2006 *Phys. Rev.* **C73** 051601(R).
- [121] Li Q et al., 2006 *J. Phys.* **G32** 151.
- [122] Lemmon RC, Russotto P et ASYEoS Collab., 2009 *Constraining the symmetry energy at suprasaturation densities with measurements of neutron and proton elliptic flows*, Exp. proposal accepted at SIS-GSI.

- [123] Serot BD, Walecka JD, 1986 *Adv. Nucl. Phys.* **16** 1
- [124] Greco V et al., 2001 *Phys. Rev.* **C64** 045203
- [125] Fuchs C, Lenske H, Wolter HH, 1995 *Phys. Rev.* **C52** 3043
- [126] Rusnak JJ, Furnstahl RJ, 1997 *Nucl. Phys.* **A627** 495
- [127] de Jong F, Lenske H, 1998 *Phys. Rev.* **C57** 3099
- [128] Alonso D, Sammarruca F, 2003 *Phys. Rev.* **C67** 054301
- [129] Typel S, van Chossy T, Wolter HH, 2003 *Phys. Rev.* **C67** 034002  
Typel S, 2005 *Phys. Rev.* **C71** 064301.
- [130] Greco V et al., 2001 *Phys. Rev.* **C63** 035202.
- [131] We use a “Minimal” Non-Linear (NL) Lagrangian, with self-interacting contributions inserted only for the isoscalar/scalar  $\sigma$  field in order to reproduce a relatively *soft* EoS for symmetric matter, in agreement with monopole and flow data.
- [132] The meson-nucleon couplings are considered not density dependent and chosen in order to reproduce good saturation properties and average Dirac-Brueckner-Hartree-Fock predictions at high density [133, 134], see details in refs.[34, 1].
- [133] Hofmann F, Keil C M and Lenske H 2001 *Phys. Rev.C* **64** 034314.
- [134] Goegelein P, van Dalen E N E, Fuchs C and Mütther H 2008 *Phys. Rev.C* **77** 025802.
- [135] Li BA, 2003 *Phys. Rev.* **C67** 017601
- [136] Aichelin J, Ko CM, 1985 *Phys. Rev. Lett.* **55** 2661
- [137] Fuchs C 2006 *Prog. Part. Nucl. Phys.* **56** 1-103.
- [138] Fuchs C. Wolter HH, 1995 *Nucl. Phys.* **A589** 732.
- [139] Prassa V et al., 2007 *Nucl.Phys.* **A789** 311.
- [140] Wolter HH, et al., 2008 *Progr. Part. Nucl. Phys.* **62** 402
- [141] Reisdorf W et al., 2007 *Nucl. Phys.* **A781** 459
- [142] Xiao Z, Li BA, Chen LW, Yong GC, Zhang M, 2009 *Phys. Rev. Lett.* **102** 062502
- [143] Trautmann W, et al., 2009 *Progr. Part. Nucl. Phys.* **62** 425
- [144] Zhao-Qing Feng, Gen-Ming Jin, 2010 *Phys. Lett.* **683** 140
- [145] Ko CM, Oh Y, Xu J, 2010 *Medium effects on charged pion ratio in HIC*, arXiv:1002.0357[nucl-th]
- [146] Cassing W, 2009 *Eur. Phys. J.* **ST168** 3
- [147] Senger P et al. 2009 *J. Phys.* **G36** 064037.
- [148] See the Website <http://nica.jinr.ru/>.
- [149] We note that our  $NL\rho$  effective Lagrangian is very close to other widely used relativistic effective models, e.g. see the  $GM3$  of ref.[150] and the  $NL3$  interaction of P.Ring and collaborators [151], which has also given good nuclear structure results, even for exotic nuclei.
- [150] Glendenning NK and Moszkowski SA, 1991 *Phys. Rev. Lett.* **67** 2414.
- [151] Vretenar D, Niksic T, Ring P., 2003 *Phys. Rev.* **C68** 024310, and refs. therein.
- [152] Chodos A et al., 1974 *Phys. Rev.* **D9** 3471.
- [153] Di Toro M, Liu B, Greco V, Baran V, Colonna M, Plumari S, 2009 *Isospin Effects on the Mixed Hadron-Quark Phase at High Baryon Density*, arXiv:0909.3247[nucl-th].
- [154] Burgio GF, Baldo M, Sahu PK, Schulze H-J 2002 *Phys. Rev.* **C66** 025802.
- [155] Nicotra OE, Baldo M, Burgio GF, Schulze H-J 2006 *Phys. Rev.* **D74** 123001.
- [156] Ozel F, Baym G, Guver T, 2010 *Astrophysical Measurement of the EoS of Neutron Star Matter*, arXiv:1002.3153[astro-ph].
- [157] Müller B, 1995 *Rep. Prog. Phys.* **58** 611.
- [158] Landau LD and Lifshitz L, 1969 *Statistical Physics* Pergamon Press, Oxford.
- [159] Stoecker H 2008, private communication.
- [160] Csernai L and Rohrich D, 1999 *Phys. Lett.* **B458** 454.
- [161] Fries RJ, Greco V and Sörensen, 2008 *Ann. Rev. Nucl. Part. Sci.* **58** 177.
- [162] Sissakian AN, Sorin AS and Toneev VD, 2008 *Phys. Part. Nucl.* **39** 1062.
- [163] Kogut JB and Sinclair DK, 2004 *Phys. Rev.* **D70** 095401.
- [164] Toublan D, Kogut JB, 2005 *Phys. Lett.* **B605** 129.

- [165] Nambu Y and Jona-Lasinio G 1961 *Phys. Rev.* **122** 345; **124** 246.
- [166] Frank M, Buballa M and Oertel M 2003 *Phys. Lett.B* **562** 221.
- [167] Buballa M 2005 *Phys. Rep.* **407** 205-376.
- [168] Guo-yun Shao et al., 2006 *Phys. Rev.* **D73** 076003
- [169] Plumari S 2009 Ph.D.Thesis, Univ.Catania.
- [170] Weise W, 2007 *Prog. Theor. Phys. Suppl.* **170** 161.
- [171] Kaiser N and Weise W, 2009 *Phys. Lett.* **B671** 25.
- [172] Pagliara G, Schaffner-Bielich J, 2010 *Phase transition from nuclear matter to color superconducting quark matter: the effect of isospin*, arXiv:1003.1017[nucl-th].